Monomeric and Dimeric Oxidomolybdenum(V and VI) Complexes, Cytotoxicity, and DNA Interaction Studies: Molybdenum Assisted C=N Bond Cleavage of Salophen Ligands

Mono- and Dimeric Oxidomolybdenum(V and VI) Complexes, Cytotoxicity, DNA Interaction Studies: Unprecedented Mo Assisted C=N Bond Cleavage of Salophen Ligands

Sudarshana Majumder,[†] Sagarika Pasayat,[†] Alok K. Panda,[§] Subhashree P. Dash,[†,‖] Satabdi Roy,[†] Ashis Biswas,[§] Mokshada E. Varma,[⊥] Bimba N. Joshi,[⊥] Eugenio Garribba,[¥] Chahat Kausar,[Ψ] Samir Kumar Patra,[Ψ] Werner Kaminsky,[‡] Aurélien Crochet,[£] Rupam Dinda [†*]

[†] Department of Chemistry, National Institute of Technology, Rourkela 769008 Odisha India

[§] School of Basic Sciences, Indian Institute of Technology Bhubaneswar, Bhubaneswar 751013, Odisha, India

[‖] Department of Basic Sciences, Paralamaharaja Engineering College, Sitalapalli, Brahmapur, Odisha 761003, India

[⊥] Bioprospecting Group, Agharkar Research Institute, G.G. Agharkar Road, Pune 411004, India

[¥] Dipartimento di Chimica e Farmacia, Università di Sassari, Via Vienna 2, I-07100 Sassari, Italy

[Ψ] Department of Life Science, National Institute of Technology, Rourkela 769008 Odisha India

[‡] Department of Chemistry, University of Washington, Box 351700, Seattle, WA 98195, USA

[£] Department of Chemistry, Fribourg Center for Nanomaterials, University of Fribourg, CH-1700 Fribourg, Switzerland

ABSTRACT

Four novel dimeric bis-μ-imido bridged metal-metal bonded oxidomolybdenum(V) complexes $[Mo^{V}{}_2O_2L'_2{}^{1-4}]$ (**1**–**4**) (where L'^{1-4} are rearranged ligands formed *in situ* from H_2L^{1-4}) and a new mononuclear dioxidomolybdenum(VI) complex $[Mo^{VI}O_2L^5]$ (**5**) synthesized from salen type N_2O_2 ligands are reported. This rare series of imido-bridged complexes (**1**–**4**) have been furnished from rearranged $H_3L'^{1-4}$ ligands, containing an aromatic diimine (*o*-phenylenediamine) 'linker', where Mo assisted hydrolysis followed by −C=N bond cleavage of one of the arms of the ligand H_2L^{1-4} took place. A monomeric molybdenum(V) intermediate species $[Mo^{V}O(HL'^{1-4})(OEt)]$ ($\mathbf{I_d^{1-4}}$) was generated *in situ*. The concomitant deprotonation of the resultant amine and dimerization of two molybdenum(V) intermediate species ($\mathbf{I_d^{1-4}}$), ultimately resulted in the formation of bis-μ-imido bridge between the two molybdenum centers of $[Mo^{V}{}_2O_2L'_2{}^{1-4}]$ (**1**–**4**). The mechanism of formation of **1**–**4** has been discussed and one of the rare intermediate monomeric molybdenum(V) species $\mathbf{I_d^4}$ has been isolated in the solid state and characterized. The monomeric dioxidomolybdenum(VI) complex $[Mo^{VI}O_2L^5]$ (**5**) was prepared from the ligand H_2L^5 where the aromatic 'linker' was replaced by an aliphatic diimine (1,2-diaminopropane). All the ligands and complexes have been characterized by elemental analysis, IR, UV–Vis spectroscopy, NMR, ESI–MS and cyclic voltammetry, and the structural features of **1**, **2**, **4** and **5** have been solved by X-ray crystallography. All the complexes (**1**–**5**) were tested for their ability to exhibit DNA binding and cleavage activity. The experimental results show that the complexes interact with CT-DNA in a manner consistent with groove binding, with binding constants ranging from 10^3–10^4 M^{-1}. All complexes show good photo-induced cleavage of pUC19 supercoiled plasmid DNA, with **4** showing the most promising photo-induced DNA cleavage activity of ~93%. Moreover, *in vitro* cytotoxic activity of all the complexes was evaluated by MTT

assay, which reveals the complexes induce cell death in MCF-7 (human breast adenocarcinoma) and HCT-15 (colon cancer) cell line.

Keywords: Salen, Oxidomolybdenum(V and VI), –C=N bond cleavage, DNA interactions, Cytotoxicity.

INTRODUCTION

The interesting coordination behavior and structural integrity of metal-metal bonded molybdenum(V) complexes make their chemistry a subject of enthusiastic research.[1,2] In the past two decades, there have been extensive studies on binuclear and polynuclear molybdenum(V) complexes containing metal-metal bonds, where molybdenum is found to be bridged through oxido,[3] sulfido,[4] telluro,[5] chloride[6] or methoxido[7] functionalities and the d-electrons of the Mo^{V} centre are localized into Mo^{V}–Mo^{V} single bonds.[8] However, examples of bis-μ-imido bridged metal-metal bonded oxidomolybdenum(V) complexes are few in literature[9] although molybdenum(V) complexes with terminal imide groups[10] have been long known.

On another hand, despite the tremendous success of platinum anticancer drugs,[11,12] there is an acute need for the development of alternative chemotherapeutic agents in cancer therapy, due to the severe side-effects and resistance phenomena of the established drugs.[13–16] Generally anticancer agents which damage or block DNA synthesis are approved for clinical use.[17] In this regard, the oxidative nature of metallo-salen complexes have encouraged biochemists to develop novel DNA/RNA modifiers and biomolecular probes.[18–21] It has been established that the DNA interaction and antiproliferative potential of the metallo-salen complexes are highly dependent on the type of the central metal ion, and the nature and position of substituents present on the salen moiety.[18,21,22] In addition, the bridging aliphatic or aromatic diimine moiety of salen type ligands has also been reported to significantly influence their cytotoxic efficiencies.[22a,22d,23]

In recent times, the studies on DNA interactions and antiproliferative activities of molybdenum complexes have gained substantial interest.[24–34] However, structural reports on oxidomolybdenum complexes with salen type ligands are few[35–37] and their pharmacological properties remain practically unexplored.

Our research group has been involved in the synthetic, structural and biological studies of transition metal complexes in the recent few years.[38] In continuation of our research, herein we have reported four novel dimeric bis-μ-imido bridged metal-metal bonded oxidomolybdenum(V) complexes $[Mo_2^{V}O_2L'^{1-4}_2]$ (**1**–**4**) (where L'^{1-4} are rearranged ligands; discussed later) and a new monomeric dioxidomolybdenum(VI) complex $[Mo^{VI}O_2L^5]$ (**5**) synthesized from salen type N_2O_2 ligands (Scheme 1). As the site specific imine reduction of salen type ligands is quite unusual in literature[39] and it has been reported that molybdenum assisted reduction of aromatic imines are more feasible than those of aliphatic imines,[40] in this work an aromatic and an aliphatic diamine were judiciously chosen for preparing ligands to study their influence on the control of molecular structure of oxidomolybdenum complexes, as well as to investigate their impact on DNA interactions and cytotoxicity studies. It was observed that during metallation with $MoO_2(acac)_2$, the salophen ligands H_2L^{1-4} containing the aromatic diimine bridges, transformed to new rearranged ligands $H_3L'^{1-4}$ (Scheme 2), through molybdenum assisted hydrolysis followed by –C=N bond cleavage of one of the arms of the salophen ligands. The corresponding molybdenum(V) intermediate $[Mo^{V}O(HL'^{1-4})(OEt)]$ ($\mathbf{I_d^{1-4}}$) was generated from an initially formed dioxidomolybdenum(VI) species $[Mo^{VI}O_2(HL^{1-4})(EtOH)(acac)]$ ($\mathbf{I^{1-4}}$) during the course of the reaction as depicted in Scheme 3 (one of the molybdenum(V) intermediate species $\mathbf{I_d^4}$ has been isolated and characterized). Finally, the molybdenum(V) intermediate ($\mathbf{I_d^{1-4}}$) underwent deprotonation and concomitant dimerization to form bis-μ-imido bridged metal-metal bonded oxidomolybdenum(V) complexes $[Mo_2^{V}O_2L'^{1-4}_2]$ (**1**–**4**). In contrast, the ligand H_2L^5 with an aliphatic imine component produced a simple dioxidomolybdenum(VI) complex $[Mo^{VI}O_2L^5]$ (**5**) where no ligand reduction took place. The key role of molybdenum in the ligand transformation can be elucidated by taking into account the reports of several other transition metal complexes[41] using similar ligands, where no such imine reduction takes place.

All the ligands and complexes have been characterized by various physicochemical techniques and the structural features of **1**, **2**, **4** and **5** have been solved by X-ray crystallography. It is relevant to mention that, to the best of our knowledge, this is the first report of some bis-μ-imido bridged dimeric oxidomolybdenum(V) complexes $[Mo_2^{V}O_2L'_2{}^{1\text{-}4}]$ (**1**–**4**) synthesised from partially reduced salophen ligands, which have been structurally characterized. All the complexes (**1**–**5**) were tested for their ability to exhibit DNA binding and cleavage activity and their *in vitro* antiproliferative activity was assayed against the MCF-7 cell line.

EXPERIMENTAL SECTION

Materials and methods. All chemicals were purchased from commercial sources and used without further purification. $[MoO_2(acac)_2]$ was prepared as described in the literature.[42] Elemental analyses were performed on a Vario ELcube CHNS Elemental analyzer and IR spectra were recorded on a Perkin-Elmer Spectrum RXI spectrophotometer. ^{1}H and ^{13}C NMR spectra were recorded with a Bruker Ultrashield 400 MHz spectrometer using $SiMe_4$ as the internal standard. Electronic spectra were recorded on a Perkin-Elmer Lamda25 spectrophotometer. Magnetic susceptibility was measured with a Sherwood Scientific AUTOMSB sample magnetometer. Conductivity was measured with a Eutech CON 700 conductivity meter. Mass spectra were recorded on a SQ-300 MS instrument operating in ESI mode. Electrochemical data were collected using CH-Instruments (Model No. CHI6003E) electrochemical analyzer. Cyclic voltammetry experiments were carried out with Pt working and auxiliary electrodes and SCE as reference electrode and TBAP as supporting electrolyte. Commercially available TBAP (tetrabutylammonium perchlorate) was properly dried and used as a supporting electrolyte for recording cyclic voltammograms of the complexes. EPR spectra were recorded from 0 to 8000 Gauss at 298 K (RT) with an X-band (9.4 GHz) Bruker EMX spectrometer equipped with an HP 53150A microwave frequency counter; the microwave frequency used was in

the range 9.40-9.41 GHz. GeneJET Plasmid Isolation Kit (Thermo Scientific, USA) was used to purify the supercoiled (SC) pUC19 DNA from *E. coli* DH5α cells. Calf thymus (CT) DNA (biochemistry grade) was purchased from SRL (India). Agarose (molecular biology grade) was purchased from Sigma Aldrich (USA). MCF-7 (human breast adenocarcinoma cell line) was procured from NCCS, Pune. Penicillin, streptomycin, DMEM and fetal bovine serum were purchased from Invitrogen and MTT from Spectrochem. Propidium Iodide was purchased from Sigma Aldrich (USA). **Caution:** Although no problems were encountered during the course of this work, attention is drawn to the potentially explosive nature of perchlorates.

Synthesis of Ligands H_2L^{1-5}. The salophen ligands, H_2L^{1-4} were prepared in good yield by the condensation of *o*-phenylenediamine with the corresponding aldehydes (salicylaldehyde (H_2L^1), *o*-vanilin (H_2L^2), 5-Bromosalicylaldehyde (H_2L^3) and 2-hydroxy-1-naphthaldehyde (H_2L^4)) in a 1:2 ratio in ethanol by a adapting a reported procedure.[43] The resulting dark orange compounds were filtered, washed with ethanol and dried over fused $CaCl_2$. H_2L^5 was synthesised by condensing 1,2-diaminopropane with *o*-vanilin as reported in literature.[44] Elemental analysis results, NMR (^{1}H and ^{13}C) and IR data for all of these verified their preparation. The ^{1}H NMR data of H_2L^{1-5} have been included in Table S1.

H_2L^1: Yield: 65%. Anal. Calcd for $C_{20}H_{16}N_2O_2$: C, 75.93; H, 5.10; N, 8.86. Found C, 75.92; H, 5.17; N, 8.81. IR (KBr pellet, cm^{-1}): 3320 ν(O–H), 1623 ν(C=N). ^{13}C NMR (100 MHz, DMSO-d_6): δ (ppm) = 164.51, 160.84, 142.72, 133.91, 132.91, 128.28, 120.21, 119.94, 119.55, 117.13.

H_2L^2: Yield: 67%. Anal. Calcd for $C_{22}H_{20}N_2O_4$: C, 70.20; H, 5.36; N, 7.44. Found C, 70.23; H, 5.34; N, 7.41. IR (KBr pellet, cm^{-1}): 3484 ν(O–H), 1611 ν(C=N). ^{13}C NMR (100 MHz, DMSO-d_6): δ (ppm) = 161.33, 157.54, 151.59, 146.37, 129.37, 127.65, 122.48, 121.67, 120.86, 118.19, 79.57.

H_2L^3: Yield: 62%. Anal. Calcd for $C_{20}H_{14}Br_2N_2O_2$: C, 50.66; H, 2.98; N, 5.91. Found C, 50.62; H, 2.95; N, 5.90. IR (KBr pellet, cm^{-1}): 3480 ν(O–H), 1611 ν(C=N). ^{13}C NMR (100 MHz, DMSO-d_6): δ (ppm) = 162.67, 159.92, 142.45, 136.15, 134.23, 128.64, 121.88, 120.11, 119.63, 110.36.

H_2L^4: Yield: 68%. Anal. Calcd for $C_{28}H_{20}N_2O_2$: C, 80.75; H, 4.84; N, 6.73. Found C, 80.71; H, 4.82; N, 6.70. IR (KBr pellet, cm^{-1}): 3488 ν(O–H), 1619 ν(C=N). ^{13}C NMR (100 MHz, DMSO-d_6): δ (ppm) = 169.06, 157.82, 138.93, 137.27, 133.46, 129.46, 128.66, 127.89, 127.34, 124.11, 121.95, 121.06, 120.17, 109.70.

H_2L^5: Yield: 64%. Anal. Calcd for $C_{19}H_{22}N_2O_4$: C, 66.65; H, 6.48; N, 8.18. Found C, 66.63; H, 6.45; N, 8.12. IR (KBr pellet, cm^{-1}): 3692 ν(O–H), 1627 ν(C=N). ^{13}C NMR (100 MHz, DMSO-d_6): δ (ppm) = 167.54, 165.68, 152.01, 151.66, 148.43, 148.37, 123.62, 123.56, 118.70, 118.61, 118.33, 118.20, 115.17, 115.04, 64.44, 63.84, 56.14, 56.02, 20.33.

Synthesis of complexes $[Mo_2^{V}O_2L'_2{}^{1-4}]$ (1–4).[a] $[MoO_2(acac)_2]$ (1 mmol) was added to a refluxing solution of the appropriate ligand H_2L^{1-4} (1 mmol) in 20 mL of ethanol; the colour initially changed to pale blue and then to dark red. The change of colour from pale blue to red was very fast for **1**–**3**, while for **4** the colour remained blue till fifteen minutes. The reflux was continued for 3 hours and filtered. A dark red residue was obtained. Red crystals of **1**, **2**, and **4** were obtained by recrystallizing the residue in DMSO. The crystals were filtered and washed with ethanol. Some of the crystals were of good quality and were suitable for X-Ray analysis. Due to the poor quality of the crystals of **3**, its X-ray structure could not be solved. Elemental analysis results, IR, NMR (^1H, ^{13}C), UV-Vis and ESI-MS data for all of the complexes verified their preparation. The ^1H NMR data of $[Mo_2^{V}O_2L'_2{}^{1-4}]$ (**1**-**4**) and $[Mo^{VI}O_2L^5]$ (**5**) have been included in Table S1.

$[Mo_2^{V}O_2L'_2{}^{1}]$(1): Yield: 34%. Anal. Calcd for $C_{26}H_{18}Mo_2N_4O_4$: C, 48.62; H, 2.82; N, 8.72. Found: C, 48.60; H, 2.81; N, 8.73. Main IR peaks (KBr, cm^{-1}): 1601 ν(C=N), 951, 855 ν(Mo=O). UV-Vis

(DMSO): λ_{max}, nm (ε, dm^3 mol^{-1} cm^{-1}): 465 (2824), 368 (6422), 320 (13313), 290 (18595). ^{13}C NMR (100 MHz, DMSO-d_6): δ (ppm) = 177.30, 172.51, 161.61, 147.74, 142.03, 137.44, 136.87, 133.79, 122.48, 121.97, 116.76, 112.23, 111.97. ESI-MS: *m/z* 642.15 $[M]^+$.

$[Mo_2^VO_2L'_2^2]$(2): Yield: 32%. Anal. Calcd for $C_{28}H_{22}Mo_2N_4O_6$: C, 47.88; H, 3.16; N, 7.98. Found C, 47.84; H, 3.12; N, 7.94. IR (KBr pellet, cm^{-1}): 1598 ν(C=N), 946, 912 ν(Mo=O). UV-Vis (DMSO): λ_{max}, nm (ε, dm^3 mol^{-1} cm^{-1}): 483 (11914), 395 (20699), 328 (46037), 275 (52678). ^{13}C NMR (100 MHz, DMSO-d_6): δ (ppm) = 155.28, 153.70, 151.87, 148.94, 134.32, 129.02, 126.17, 122.34, 118.89, 118.21, 116.53, 115.70, 115.57, 55.74. ESI-MS: *m/z* 702.16 $[M]^+$.

$[Mo_2^VO_2L'_2^3]$ (3): Yield: 35%. Anal. Calcd for $C_{26}H_{16}Br_2Mo_2N_4O_4$: C, 39.03; H, 2.02; N, 7.00. Found C, 39.01; H, 2.00; N, 7.02. IR (KBr pellet, cm^{-1}): 1597 ν(C=N), 911, 883 ν(Mo=O). UV-Vis (DMSO): λ_{max}, nm (ε, dm^3 mol^{-1} cm^{-1}): 484 (9759), 383 (17993), 276 (57553). ^{13}C NMR (100 MHz, DMSO-d_6): δ (ppm) = 162.90, 154.61, 152.45, 137.33, 136.86, 134.63, 129.94, 124.63, 121.76, 119.02, 116.30, 116.22, 110.88. ESI-MS: *m/z* 800.64 $[(M–H)^+]$.

$[Mo_2^VO_2L'_2^4]$(4): Yield: 26%. Anal. Calcd for $C_{34}H_{22}Mo_2N_4O_4$: C, 55.00; H, 2.99; N, 7.55. Found C, 55.02; H, 2.94; N, 7.52. IR (KBr pellet, cm^{-1}): 1565 ν(C=N), 937, 912 ν(Mo=O). UV-Vis (DMSO): λ_{max}, nm (ε, dm^3 mol^{-1} cm^{-1}): 486 (15710), 397 (17833), 349 (30945), 279 (55015). ^{13}C NMR (100 MHz, DMSO-d_6): δ (ppm) = 193.30, 169.13, 157.79, 138.91, 138.86, 137.30, 133.46, 129.47, 129.30, 128.66, 127.89, 127.32, 124.72, 124.11, 121.98, 121.07, 109.68. ESI-MS: *m/z* 742.28 $[M]^+$.

[a] In an alternative strategy, when the synthesis of the complexes **1**–**4**, was carried out in presence of few drops of acetic acid, the yield of the complexes increased significantly.

Synthesis of the intermediate species $[Mo^VO(HL'^{1\text{-}4})(OEt)]$ (**I_d^4**).[b] $[MoO_2(acac)_2]$ (1 mmol) was added to a refluxing solution of H_2L^4 (1 mmol) in ethanol. The solution turned pale blue and the

reaction was stopped after fifteen minutes when the solution was still blue and filtered. Blue residue of $\mathbf{I_d^4}$ was obtained. Elemental analysis results, IR, UV-Vis, EPR and ESI-MS data for the complex verified its preparation. The corresponding intermediates $[Mo^{V}O(HL'^{1\text{-}3})(OEt)]$ ($\mathbf{I_d^{1\text{-}3}}$), could not be isolated because of their very fast conversion into the dimeric species $[Mo_2{}^{V}O_2L'_2{}^{1\text{-}3}]$ (**1**–**3**).

$[Mo^{V}O(HL'^{1\text{-}4})(OEt)]$ ($\mathbf{I_d^4}$) Yield: 15%. Anal. Calcd for $C_{19}H_{17}MoN_2O_3$: C, 54.69; H, 4.11; N, 6.71;. Found C, 54.64; H, 4.10; N, 6.73. IR (KBr pellet, cm^{-1}): 946 (Mo=O), 1564 (–C=N), 1620 (–C=O). UV-Vis (DMSO): λ_{max}, nm (ε, $dm^3\ mol^{-1}\ cm^{-1}$): 607 (4692), 562 (2917), 523(1466), 323(14222), 274(46436). ESI MS: *m/z* 421.64 $[(M+2H)^+]$.

[b]In an alternative strategy, when $[MoO_2(acac)_2]$ (1 mmol) was added to a refluxing solution of H_2L^4 (1 mmol) in ethanol in presence of few drops of water, the solution remained blue for 30 minutes and blue residue of $\mathbf{I_d^4}$ was now obtained in a higher yield.

Synthesis of $[Mo^{VI}O_2L^5]$ (5). [$MoO_2(acac)_2$] (1 mmol) was added to a refluxing solution of H_2L^5 (1 mmol) in 20 mL of ethanol; the colour changed to orange. The solution was refluxed for 3 hours. Dark orange crystalline residue of **5** was obtained on filtering the solution. Some of the crystals were of good quality and were used directly for X-Ray analysis. Elemental analysis results, IR, NMR (^1H, ^{13}C), UV-Vis and ESI-MS data for the complex verified its preparation.

$[Mo^{VI}O_2L^5]$(5): Yield: 42%. Anal. Calcd for $C_{19}H_{20}MoN_2O_6$: C, 48.73; H, 4.30; N, 5.98. Found C, 48.71; H, 4.29; N, 5.94. IR (KBr pellet, cm^{-1}): 1607 ν(C=N), 907, 874 ν(Mo=O). UV-Vis (DMSO): λ_{max}, nm (ε, $dm^3\ mol^{-1}\ cm^{-1}$): 438 (1871), 323 (7254), 278 (12155). ^{13}C NMR (100 MHz, DMSO-d_6): δ (ppm) = 164.21, 159.45, 150.85, 150.71, 149.61, 148.93, 132.08, 129.14, 126.65, 126.29, 124.98, 124.47, 123.62, 123.55, 122.39, 121.74, 121.67, 121.60, 121.29, 118.72, 118.64, 118.34, 118.20, 117.68, 117.24, 116.91, 116.78, 116.54, 115.18, 115.05, 67.85, 64.51, 63.90, 62.64, 38.51, 30.24, 28.82, 22.87. ESI-MS: *m/z* 468.12 $[M]^+$.

Crystallography. Clear inclusion free single crystals of **1**, **2**, **4** and **5** suitable for X-ray diffraction studies, were mounted on loops with oil. Crystallographic data and details of refinement are given in Table 1. The compounds **1, 2**, and **5** crystallize in the triclinic space group $P\overline{1}$, and **4** crystallizes in monoclinic space group P 2_1/n. The unit cell parameters and the intensity data were collected for complexes **1** and **2** on a Bruker APEX II using graphite monochromated Mo Kα radiation (λ = 0.71073 Å) at ~110 K and ~100 K respectively. The data for complex **4** were collected on SuperNova AS2 Data Collections using high intensity of SuperNova microfocus Cu Kα source (λ = 1.54184 Å) and a highly sensitive Atlas CCD detector at ~ 100 K. Single crystals of complex **5** were mounted on a Stoe IPDS 2 diffractometer equipped with an Oxford Cryosystem open flow cryostat using a graphite monochromated Mo Kα radiation (λ = 0.71073 Å) at ~ 200 K. The intensity data were corrected for Lorentz, polarization and absorption effects. The data was integrated and scaled using SAINT, SADABS within the APEX2 software package by Bruker.[45a] The structures were solved using the SHELXS97[45b] and refined using SHELXL97[46] computer programs. Hydrogen atoms were placed in geometrically idealized positions and constrained to ride on their parent atoms with C–H distances in the range 0.95–1.00 Å. Isotropic thermal parameters U_{eq} were fixed such that they were $1.2U_{eq}$ of their parent atom Ueq for CH's and $1.5U_{eq}$ of their parent atom U_{eq} in case of methyl groups. All non-hydrogen atoms were refined anisotropically by full-matrix least-squares.

Table 1. Crystal data and refinement data of complexes **1**, **2**, **4** and **5**.

Compound	**1**	**2**	**4**	**5**
Formula	$C_{26}H_{18}Mo_2N_4O_4$	$C_{28}H_{22}Mo_2N_4O_6$	$C_{34}H_{22}Mo_2N_4O_4$	$C_{19}H_{20}MoN_2O_6$
M	642.32	702.38	742.44	468.31
Crystal symmetry	Triclinic	Triclinic	Monoclinic	Triclinic
Space group	$P\bar{1}$	$P\bar{1}$	$P\ 2_1/n$	$P\bar{1}$
a (Å)	8.5389(13)	9.4562(5)	8.9152(3)	11.9576(11)
b (Å)	10.4521(14)	9.6471(5)	17.7572(6)	12.8243(13)
c (Å)	13.565(2)	14.4626(7)	17.7893(6)	13.8984(14)
α (°)	88.732(9)	79.619(2)	90	76.348(8)
β (°)	80.213(9)	79.536(3)	104.473(3)	77.430(8)
γ(°)	70.999(9)	88.060(2)	90	78.140(8)
V (Å^3)	1127.3(3)	1276.17(11)	2726.84(16)	1994.6 (3)
Z	2	2	4	4
D_{calc} (g cm^{-3})	1.892	1.828	1.808	1.556
μ(Mo-Kα) (mm^{-1})	1.156	1.036	7.948	0.695
F(000)	636	700	1480	952
max./min.trans.	0.988 / 0.893	0.9597 / 0.9125	0.933 / 0.793	0.933 / 0.793
θ (max) (°)	26.77	28.36	73.97	25.00
Temperature (K)	110	100	100	200
Reflections collected	10634	54801	8414	9605
R^a [I>2σ(I)]	0.0538	0.0250	0.0487	0.0513
Rw^b [all data]	0.1103	0.0629	0.1336	0.1035
S [goodness of fit]	0.974	1.062	1.040	0.826
max./min. res. (e Å^{-3})	0.914 / -0.895	0.658 / -0.670	1.549 / -0.662	0.483 / -0.692

[a] $R=\frac{\Sigma||Fo|-F|c||}{\Sigma||Fo|-F|c||}$

[b] $R_w=\sqrt{\Sigma[w(F_o^{\,2}-F_c^{\,2})]\Big/\Sigma[w(F_o^{\,2})^2]}$

DNA binding experiments

Using absorption spectroscopy. The binding of the dimeric oxidomolybdenum(V) and monomeric dioxidomolybdenum(VI) complexes to calf thymus DNA (CT-DNA) was examined as previously described.[38c-g] Briefly, the UV-Vis titration experiments were carried out with variable CT-DNA concentrations (0–50 μM) against a fixed concentration of molybdenum complex (25 μM) in 10 mM Tris–HCl buffer (pH 8.0) containing 1% DMF using a Lambda 35, Perkin-Elmer (USA) spectrophotometer. The binding of ligands to CT-DNA were also studied. To do this the concentration of ligand was fixed at 25 μM and was titrated with variable DNA concentration (0–250 μM) in 10 mM Tris–HCl buffer (pH 8.0) containing 1% DMF. The data obtained from the titration experiments were then fit to the following equation to obtain binding constant K_b:[38c-g]

$$\frac{[DNA]}{\varepsilon_a-\varepsilon_f} = \frac{[DNA]}{\varepsilon_b-\varepsilon_f} + \frac{1}{K_b(\varepsilon_b-\varepsilon_f)} \quad \text{(Eq. 1)}$$

where [DNA] is the concentration of DNA base pairs, ε_a, ε_f and ε_b correspond to apparent extinction coefficient for the complex *i.e*. Abs/[complex] in the presence of DNA, in absence of DNA and to fully bound DNA, respectively. A plot of $[DNA]/(\varepsilon_a - \varepsilon_f)$ *vs* [DNA] gave a slope and intercept equal to $1/(\varepsilon_b - \varepsilon_f)$ and $1/K_b(\varepsilon_b - \varepsilon_f)$, respectively; K_b is calculated from the ratio of the slope to the intercept.

Using thermal denaturation technique. Thermal denaturation studies of CT-DNA (100 μM) in the absence and presence of molybdenum complexes (25 μM) were carried out by monitoring the absorbance at 260 nm in the temperature range of 30–90 ^oC in 10 mM Tris-HCl buffer (pH 8.0) containing 1% DMF. The ramp rate for each of the experiment was 0.5 ^oC/min. All the experiments were carried out in absorbance mode using a Chirascan CD spectropolarimeter (Applied Photophysics, UK) equipped with a peltier temperature controller. The melting temperature (T_m) was calculated from the derivative plot (dA_{260}/dT *vs* T) of the melting profile.[47a]

Using Circular dichroism spectroscopy. Circular Dichroism (CD) spectroscopy was studied using Chirascan CD spectropolarimeter (Applied Photophysics, UK) at 25 ^{o}C. CD spectra of CT-DNA (100 μM) in the absence and presence of molybdenum complexes (25 μM) were obtained in the wavelength range of 240–400 nm in 10 mM Tris-HCl buffer (pH 8.0) containing 1% DMF using quartz cell with 10 mm path length.[38c-g]

Fluorescence experiments. The fluorescence spectra of the complexes **1**–**5** (100 μM) as well as ligands (100 μM) in 10 mM Tris-HCl buffer (pH 8.0) containing 1% DMF at 25 °C were recorded using a spectrofluorimeter using Fluoromax 4P (Horiba Jobin Mayer, USA). The excitation wavelength was set to 355 nm and the emission spectra were recorded between 370–600 nm. Data were collected at 0.5 nm wavelength resolution using quartz cell with 10 mm path length.

DNA cleavage experiments. For DNA cleavage experiments, 300 ng supercoiled (SC) pUC19 DNA was used and all experiments were carried out in 50 mM Tris-HCl buffer (pH 8.0) containing 1% DMF.

Chemical-induced DNA cleavage. For chemical nuclease studies, the cleavage experiments were carried out in dark using hydrogen peroxide (0.5 mM) as the oxidising agent in the absence and presence of the molybdenum complexes (1–100 μM). The reactions were incubated at 37 °C for 3 h and analysed for DNA cleaved products by agarose gel electrophoresis.

Photo-induced DNA cleavage. The photo-induced DNA cleavage studies were done as described previously.[38c-g] Briefly, the photolytic DNA cleavage experiments were carried out on supercoiled (SC) pUC19 DNA (300 ng) with molybdenum complexes (1–100 μM) in 50 mM Tris HCl buffer (pH 8.0) containing 1% DMF. The extent of DNA cleavage was measured from the intensities of the bands using the UVP Gel Documentation System (Gel Doc It^2). The observed error in measuring the band intensities ranged between 3–6%. The mechanistic aspect behind the DNA cleavage was also studied using four different additives: two singlet oxygen quenchers (sodium azide and L-histidine)

and other two hydroxyl radical quenchers (KI and D-mannitol). These additives were added to the reaction mixture prior to the addition of the complex. The concentration of each additive was 0.5 mM.

Cytotoxicity Studies

MTT Assay. MCF-7 cells were cultured in DMEM containing 10% FBS and penicillin (100U/ml) and streptomycin (100 µg/ml) in a humidified 5% CO_2 incubator at 37 °C. The cytotoxicity was assayed by determining the viability of MCF cells after treatment by MTT assay. Briefly, MCF-7 cells (10^5 cells/well) were seeded in 96 well plates in DMEM containing 10% FBS. After cells reached confluency, treatment was given with varying concentrations (5 µM, 10 µM, 25 µM and 50 µM) of the molybdenum complexes. The complexes were dissolved in DMSO and working solutions were prepared by diluting the stock of 5 mM of each compound with plain DMEM. Final working concentration of DMSO in assay was less than 2%. Untreated cells were taken as 100% survival. After the treatment, medium was removed and cells were incubated with MTT (5 mg/mL) for 4 hours. The crystals formed were dissolved in DMSO and absorbance was read at 570 nm. IC_{50} was calculated for each compound by treating the cells for 48 h.

Propidium Iodide Staining. Propidium Iodide (or PI) is an intercalating agent which has the fluorescence excitation maximum is 535 nm and the emission maximum is 617 nm.[47b] PI staining was performed to visualize the morphology of the nuclei after the treatment with molybdenum complexes. The MCF-7 (Human breast cancer cells) cells were grown in the 96-well plate. After reaching approximately 90% confluency, the cells were treated with molybdenum complexes at different concentrations (5, 10, 25, 50 µM) and were incubated for 48 hours. Cells were observed under inverted fluorescence microscope after treatment to check for morphological changes, during cell death. Then the cells were washed twice with PBS (pH 7.4) and fixed after incubation for 15 min with 3.7 % of formaldehyde. After that, the cells were again washed twice with PBS and treated with 0.2% triton-X 100 in PBS for 30 seconds. Again the cells were washed twice with PBS and PI solution (10

μg/mL) was added and kept for 15 min in dark. Finally the cells were washed twice with PBS and imaged under fluorescence microscope (FLoid, Life technologies).

RESULTS AND DISCUSSION

Synthesis. Scheme 1 portrays the synthesis of four dimeric oxidomolybdenum(V) complexes $[Mo_2^{V}O_2L'_2{}^{1-4}]$ (**1**–**4**), where L'^{1-4} indicates the rearranged form of the ligands H_2L^{1-4}, and a monomeric dioxidomolybdenum(VI) complex (**5**), via two different reaction pathways (path a and path b), from salen type ligands (H_2L^{1-5}).

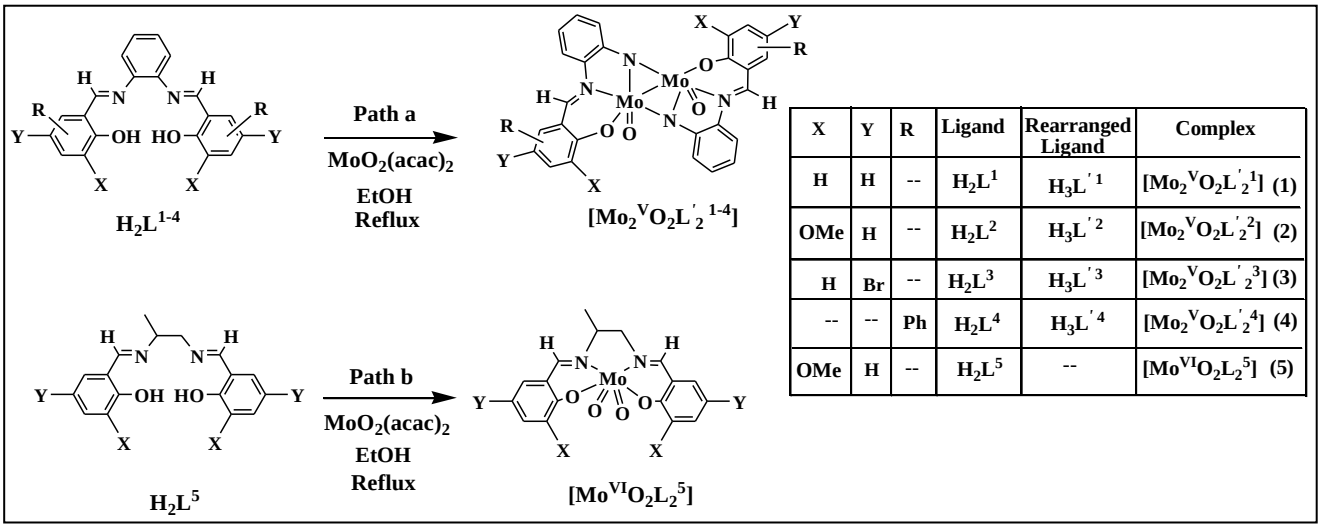

X	Y	R	Ligand	Rearranged Ligand	Complex
H	H	--	H_2L^1	$H_3L'^1$	$[Mo_2^{V}O_2L'_2{}^1]$ (1)
OMe	H	--	H_2L^2	$H_3L'^2$	$[Mo_2^{V}O_2L'_2{}^2]$ (2)
H	Br	--	H_2L^3	$H_3L'^3$	$[Mo_2^{V}O_2L'_2{}^3]$ (3)
--	--	Ph	H_2L^4	$H_3L'^4$	$[Mo_2^{V}O_2L'_2{}^4]$ (4)
OMe	H	--	H_2L^5	--	$[Mo^{VI}O_2L_2^5]$ (5)

Scheme 1. Synthesis of dimeric oxidomolybdenum(V) complexes $[Mo_2^{V}O_2L'_2{}^{1-4}]$ (**1**–**4**) and monomeric dioxidomolybdenum(VI) complex $[Mo^{VI}O_2L^5]$ (**5**).

When the ligands were subjected to reflux in presence of $MoO_2(acac)_2$, H_2L^{1-4} (which contained the aromatic diimine) followed the reaction path 'a' (Scheme 1) which involved a Mo(V) intermediate, $[Mo^{V}O(HL'^{1-4})(OEt)]$ (**I_d^{1-4}**) and finally dimeric bis-μ-imido bridged oxidomolybdenum(V) complexes $[Mo_2^{V}O_2L'_2{}^{1-4}]$ (**1**–**4**) were formed, containing rearranged ligands $H_3L'^{1-4}$ furnished by Mo assisted –C=N bond reduction (Scheme 2). One of the intermediates, **I_d^4**, has been isolated in the solid state and characterized by UV-Vis, IR, EPR spectroscopy and ESI-MS.

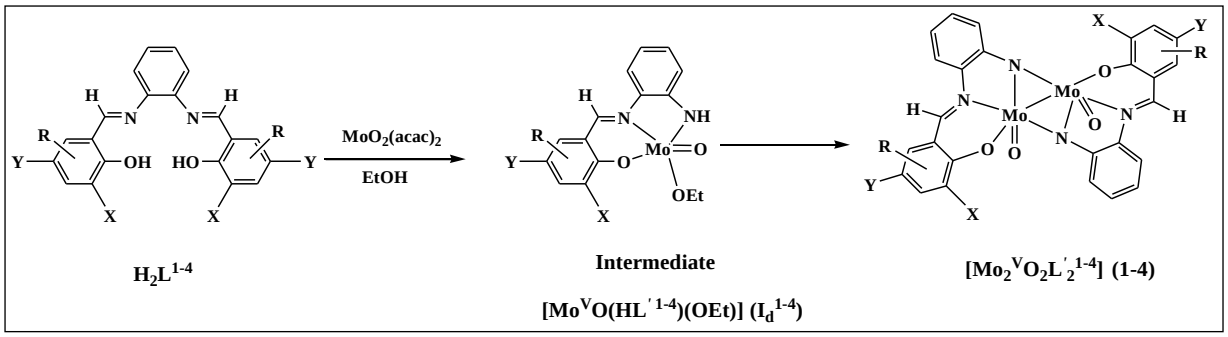

Scheme 2. Schematic pathway for the formation of $[Mo_2^{V}O_2L'^{1-4}_2]$ (**1–4**) via the intermediate $[Mo^{V}O(HL'^{1-4})(OEt)]$ ($\mathbf{I_d^{1-4}}$).

The detailed mechanism of the formation of $[Mo_2^{V}O_2L'^{1-4}_2]$ (**1–4**) is shown in Scheme 3, taking H_2L^2 as a representative among the four ligands, which illustrates that at first a dioxidomolybdenum(VI) species $[Mo^{VI}O_2(HL^2)(acac)(EtOH)]$ ($\mathbf{I^2}$) is formed, and then a molybdenum assisted hydrolysis of one of the coordinated –C=N bond of the salophen ligand takes place to form $\mathbf{I_a}^2$ which releases Hacac[47c] and $\mathbf{I_b}^2$ is formed. The pendant phenolic OH then coordinates to the metal centre and removal of the aldehyde (*o*-vanilin) as an acid (*o*-vanillic acid)[47d] takes place *in lieu* of the reduction of Mo(VI) species ($\mathbf{I_b}^2$) to Mo(IV) species ($\mathbf{I_c}^2$). The Mo(IV) species, $\mathbf{I_c}^2$, then undergoes a fast comproportionation[47e] reaction with a Mo(VI) species present in the reaction medium to form a Mo(V) intermediate $\mathbf{I_d}^2$**.** Finally the dimerization of $\mathbf{I_d}^2$ occurs with the loss of ethanol and μ-imido bridges between two molybdenum fractions is furnished to yield $[Mo_2^{V}O_2L'^{2}_2]$ (**2**).

The reaction may also follow an alternative pathway (Scheme S1), where the Mo(VI) species can undergo an oxidative deamination[47f-i] *in lieu* of the reduction of Mo(VI) species to Mo(IV) species with the release of one of the oxido oxygen as water.[47j,k] $[Mo_2^{V}O_2L'^{2}_2]$ (**2**) is then formed following the similar steps described in Scheme 3.

In the above reaction, H^+ ion plays a significant role (it is assumed that the source of H^+ ion was from free acetylacetone generated from the metal precursor $MoO_2(acac)_2$ in solution). In fact, when the same reaction is carried out in an acidic medium (with few drops of acetic acid), it has been found that the yield of **2** increases drastically from 32% to 94%, which supports the fact that the reaction is acid catalysed. There are reports of vanadium complexes of similar ligands where such imine reduction did not take place in the presence of $VO(acac)_2$ (Scheme 3).[41a,b] It has also been found in literature that in presence of several other transition metals (Ti,[41c] Cr,[41d] Mn,[41e] Fe,[41f] Co,[41g] Ni,[41h] Cu,[41i] Zn,[41j] W,[35c] Os,[41k] and Pt[41l]), –C=N bond cleavage of salophens does not take place, which proves that the hydrolysis and −C=N bond cleavage of salophens in complex **1**–**4** is molybdenum assisted. X-ray crystallography (discussed later) revealed the presence of a localized metal-metal single bond between the two molybdenum(V) centers of all the oxidomolybdenum(V) complexes $[Mo_2^{V}O_2L'_2{}^{1\text{-}4}]$ (**1**–**4**). The formation of the monomeric dioxidomolybdenum(VI) complex $[Mo^{VI}O_2L^5]$ (**5**) took place via path 'b' (Scheme 1) where no such hydrolysis and −C=N bond cleavage of H_2L^5 occurred in presence of $MoO_2(acac)_2$ owing to the fact that, during the –C=N bond cleavage, the corresponding intermediate $[Mo^{VI}O_2(HL'^{1\text{-}4})(EtOH)(acac)(H_2O)]$ ($\mathbf{I_b}^5$), would not get any resonance stabilization due to the absence of aromatic backbone in the ligand environment, which is available in case of $\mathbf{I_b}^{\mathbf{1\text{-}4}}$.

All the complexes **1**–**5** were completely soluble in DMF, DMSO and partially soluble in CH_3CN, CH_2Cl_2 and H_2O. The complexes were stable in both solid and solution phases. The solution phase stability of the complexes over the period of the biological assays, i.e. 72 h, was confirmed by electronic absorption and NMR studies (Figure S1). Magnetic susceptibility and molar conductivity data indicate that all the complexes (**1**–**5**) are diamagnetic and electrically non-conducting in solution. The oxidomolybdenum(V) complexes (**1**–**4**) are silent in Electron Paramagnetic Resonance (EPR)

spectroscopy which may be attributed to the antiferromagnetic coupling[48a] of electron spins of the two $4d^1$ Mo(V) ions and the formation of an Mo–Mo bond.[1,3i,48b,c]

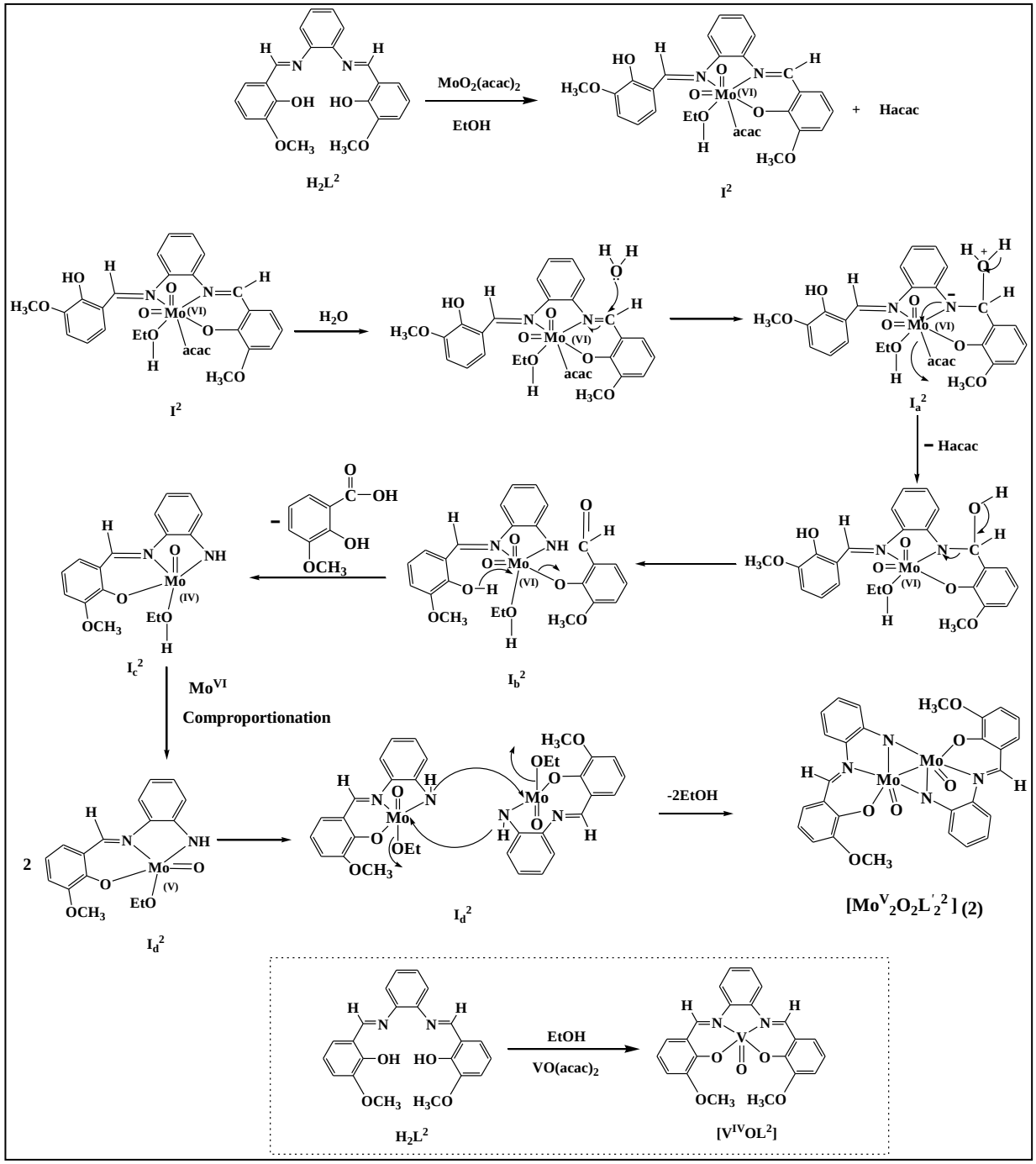

Scheme 3. Proposed mechanistic pathway of formation of dimeric oxidomolybdenum(V) complex $[Mo_2{}^{V}O_2L'_2{}^{2}]$ (**2**) and corresponding oxidovanadium(IV) complex, $[V^{IV}OL^2]$.[41a,b]

IR Spectroscopy. Selected IR data of all the ligands ($H_2L^{1–5}$) and the complexes **1**–**5** are given in the *Experimental Section*. The ligands exhibit the IR band of minimum intensity in the 3320–3692 cm^{-1} region due to *v*(OH) stretching.[43] Distinct bands within the range of 1611–1627 cm^{-1} due to *v*(C=N) of azomethine groups of the salen type ligands[32,43] ($H_2L^{1–5}$) were noticed. In the complexes (**1**–**5**), the *v*(C=N) stretching was shifted to lower frequencies (1565–1607 cm^{-1}) which might be attributable to the lower C=N bond order due to the coordination to the metal atom.[33] In addition, the complexes **1**–**5** display a pair of sharp strong peaks in the range 855–946 cm^{-1} due to *v*(M=O) stretch.[49a,b,c] The intermediate [$Mo^{V}O(HL'^{4})(OEt)$] (**I_d^4**), which has been isolated, showed a strong oxido peak at 946 cm^{-1} due to a single *v*(M=O) stretch.[49a,b,c] A sharp absorption at 1620 cm^{-1} is observed which can be attributed to the stretching of –C=O of the coordinated acetylacetone, while the peak at 1564 cm^{-1} is due to the –C=N stretching of the imine bond of the salophen ligand.[38a] Representative spectra of complex **4** and its corresponding intermediate **I_d^4** are given in Figure S2.

UV-Vis Spectroscopy. The electronic absorption spectra of the complexes **1**–**5** were recorded in DMSO and are quite similar for all four complexes. The spectral data are summarized in the *Experimental Section*. The spectra display a shoulder in the 438–486 and two strong absorptions in the 275–395 nm range which are assignable to LMCT and intra-ligand transitions, respectively.[49a,b,c] The absorption spectrum of [$Mo^{V}O(HL'^{4})(OEt)$] (**I_d^4**), exhibits peaks at 608, 562 519, 323 and 274 nm. The band at 323 and 274 nm is attributed to the intra ligand charge transfer band, the bands at 562 and 519 nm are assigned as LMCT bands, while the peak at 607 nm is due to a d-d transition.[49d,e,f] The representative spectra of complex **4** and **I_d^4** are given in Figure S3.

NMR Spectroscopy. ^{1}H and ^{13}C NMR of all the compounds were recorded in DMSO-d_6. The ^{1}H NMR data are collected in Table S1 and the ^{13}C NMR data are given in the experimental section. The coordinating modes of $H_2L^{1–5}$ were confirmed by comparing their ^{1}H NMR spectral patterns with

those of the corresponding complexes. The representative ^{1}H NMR spectra of H_2L^2, $[Mo_2{}^{V}O_2L'_2{}^{2}]$ (**2**) and $[Mo_2{}^{V}O_2L'_2{}^{3}]$ (**3**) is given in Figures S4(a), S4(b) and S5, respectively. The ^{1}H NMR spectrum of the free ligands exhibits resonance in the range δ = 12.96–15.13 ppm due to phenolic OH and at δ = 8.52–9.68 ppm due to the azomethine –CH protons respectively.[50a] The aromatic protons from ligands are clearly observed in the expected region δ = 6.75–8.54 ppm. Singlets for the $-OCH_3$ protons of H_2L^2 and H_2L^5 are observed at around 3.74 ppm. The aliphatic protons of H_2L^5 appear as two doublets at 3.73 and 1.31 ppm for $-CH_2$ and $-CH_3$ respectively and a multiplet is observed at 3.77 ppm for –CH proton.[50] In the NMR spectra of complexes, the peak for the aromatic –OH proton disappeared due to the deprotonation of phenolic group. The NMR spectra of complex **5** exhibits double the number of protons due to the presence of two entities in one unit.

In the ^{13}C NMR spectra of the ligands H_2L^{1-5}, spectral signals for the aromatic carbons are found in the downfield region in the range δ = 109.70–169.06 ppm.[50b] The signals for the aliphatic carbons of H_2L^5 are found in the range of δ = 20.33–64.44 ppm and the signal for $-OCH_3$ of H_2L^2 appears at 79.57 ppm and the signals for $-OCH_3$ carbon and aliphatic carbons of H_2L^2 and H_2L^5 appear in the range of δ = 22.87–67.85 ppm. While in the ^{13}C NMR spectra of complexes **1**–**5**, signals for the aromatic carbons are found in the downfield region in the range δ = 109.68–193.30 ppm.[50] Figure S6 shows the ^{13}C NMR spectrum of **3**.

ESI-MS. ESI-MS spectra of **1**–**5** and $\mathbf{I_d}^{\mathbf{4}}$ have been recorded in DMSO. The characteristic molecular ion peak for **1**–**5** appear at 642.15 $[M]^+$, 702.16 $[M]^+$, 800.64 $[(M-H)^+]$, 742.28 $[M]^+$ and 468.12 $[M]^+$, respectively, while the molecular ion peak for $\mathbf{I_d}^{\mathbf{4}}$ appears at 421.64 $[(M+2H)^+]$. The representative ESI-MS spectra of $\mathbf{I_d}^{\mathbf{4}}$ and **3** are given in Figure 1 and Figure S7 respectively.

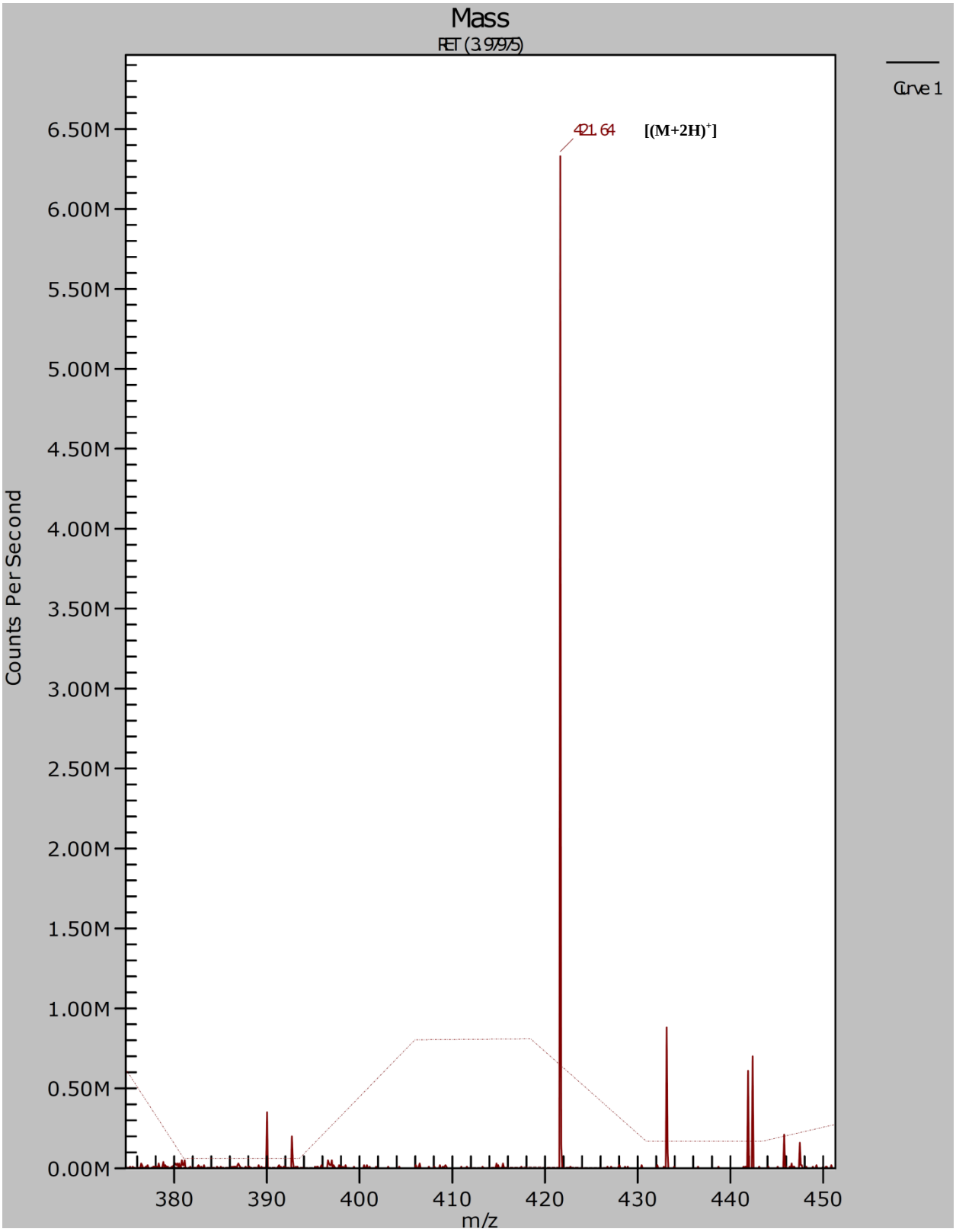

Figure 1. ESI-MS spectrum of $[Mo^{V}O(HL'^{4})(OEt)]$ ($\mathbf{I_d}^{\mathbf{4}}$).

EPR spectroscopy of the intermediate monomeric Mo(V) compound $[Mo^{V}O(HL'^{4})(OEt)]$ ($\mathbf{I_d^4}$). EPR spectra were recorded at room temperature (298 K) as function of the time on the powder compound $\mathbf{I_d^4}$ (Schemes 2 and 3), dissolved in a degassed DMSO solution. These are shown in Figure 2. The spectra consist of a strong central signal due to the coupling between an unpaired electron with the non-magnetic nuclei ^{92}Mo, ^{94}Mo, ^{96}Mo, ^{98}Mo, and ^{100}Mo (I = 0; total natural abundance 74.5%) and six hyperfine lines due to the coupling with ^{95}Mo and ^{97}Mo nuclei (I = 5/2; total abundance 25.5%), indicated by the asterisks in Figure 2. No signals below 3250 Gauss and above 3650 Gauss were revealed. These features demonstrate that the oxidation state of Mo is +V with only one electron in the 4*d* orbitals (configuration $4d^1$).[51a] The examination of the EPR spectra indicate the presence of only one species in the organic solution ($\mathbf{I_d^4}$), characterized by g_{iso} = 1.955 and A_{iso} = 40.4 × 10^{-4} cm^{-1}. These spin Hamiltonian parameters are consistent with a $Mo(N_2\text{^}O_2)$ equatorial coordination mode,[51b] and fall in the range expected by the correlation between g_{iso} and A_{iso} proposed some years ago by Enemark and co-workers.[51c]

As it can be observed, the spectral signals decrease significantly in the time range 0–26 min (at t = 26 min only the central absorption is detected and the signal to noise ratio is very low) and disappear completely for time longer than 30 min, suggesting a probable antiferromagnetic[48a] coupling between the unpaired electrons of the Mo(V) centers in the bis-μ-imido bridged oxidomolybdenum(V) complex (**4**) formed upon the dimerization of two intermediate $\mathbf{I_d^4}$ species (Scheme 3).

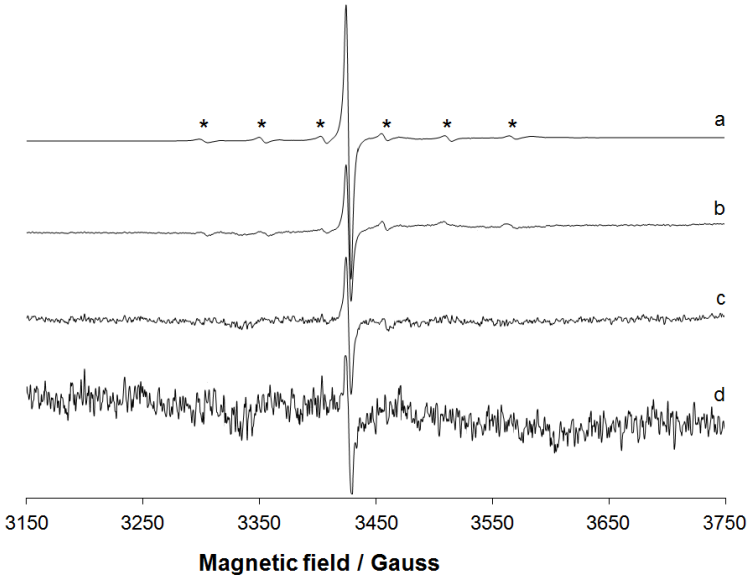

Figure 2. EPR spectra recorded at 298 K as function of the time on $\mathbf{I_d}^{\mathbf{4}}$ dissolved in a degassed DMSO solution: (a) t = 7 min; (b) t = 14 min; (c) t = 20 min; (d) t = 26 min. With the asterisks the six hyperfine lines due to the coupling between the unpaired electron with ^{95}Mo and ^{97}Mo nuclei are indicated.

Electrochemical properties. Electrochemical properties of the complexes **1**–**5** have been studied by cyclic voltammetry in DMF solution and that of $\mathbf{I_d}^{\mathbf{4}}$ has been studied in DMSO (0.1 M TBAP). The CV traces of all the binuclear oxidomolybdenum(V) complexes $[Mo_2{}^{V}O_2L'_2{}^{1\text{-}4}]$ (**1**–**4**) are of similar pattern and a representative voltammogram of $[Mo_2{}^{V}O_2L'_2{}^{4}]$ (**4**) is discussed herein. The redox potentials of all the complexes are summarized in Table 2. It is observed that **4** exhibits a single electron quasi-reversible reductive response at $E_{1/2}$ value of –0.63 V and an irreversible reductive response at –1.37 V (Figure 3(a)) which can be assigned to the reduction of Mo(V)→Mo(IV) of the two corresponding molybdenum centers.[52] Further, two single electron quasi-reversible oxidative responses at $E_{1/2}$ value of 0.78 V and 1.14 V can be attributed to the oxidation of Mo(V)→Mo(VI) in the binuclear species.

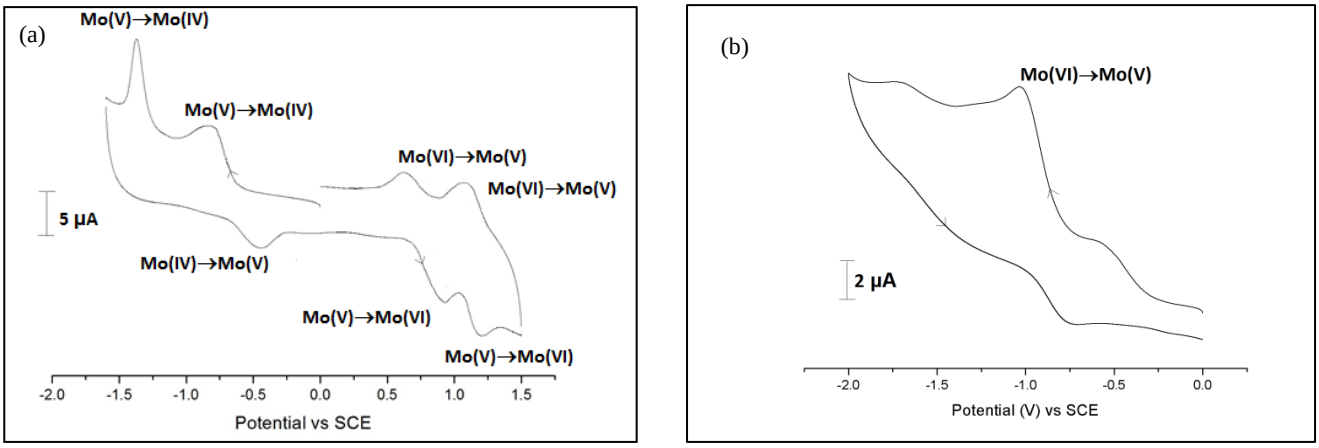

Figure 3. Cyclic voltammograms of: (a) [$Mo_2^{V}O_2L'_2{}^{4}$] (**4**), (b) [$Mo^{VI}O_2L^{5}$] (**5**).

In the CV trace of the monomeric dioxidomolybdenum(VI) complex [$Mo^{VI}O_2L^{5}$] (**5**), a single electron quasi-reversible response at $E_{1/2}$ value of –0.89 V and an irreversible reductive response at –1.69 V are observed (Figure 3(b)). The response at $E_{1/2}$ = –0.89 V can be attributed to the Mo(VI)→Mo(V) reduction, while the peak at –1.69 V is due to the reduction of the salen type ligand.[53a]

CV trace of $\mathbf{I_d^4}$ (Figure 4) shows a single electron quasi-reversible reductive response at $E_{1/2}$ value of –0.91 V due to the reduction of Mo(V)→Mo(IV).[53b,c] Another single electron quasi-reversible oxidative response at $E_{1/2}$ value of 1.04 V is observed, which can be attributed to the oxidation of Mo(V)→Mo(VI).[53b,c] The redox potentials are metal centered as the ligand does not show any reduction potential in the same potential window.[53d]

Single electron processes were verified by comparing its current height with that of the standard ferrocene–ferrocenium couple under identical experimental conditions.

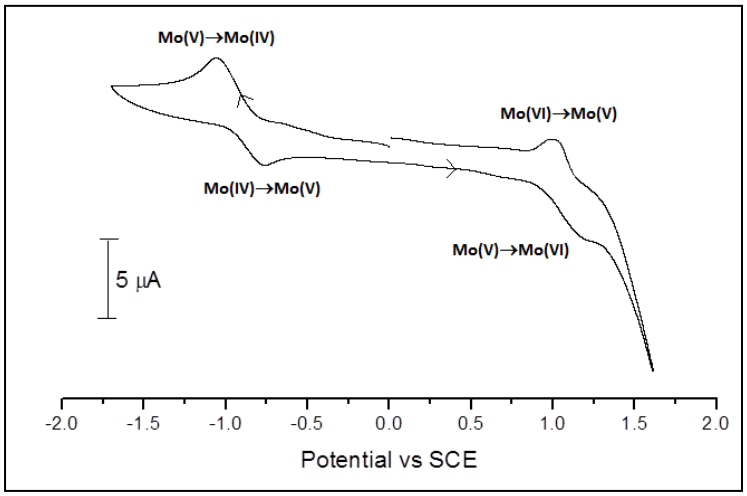

Figure 4. Cyclic voltammogram of $[Mo^{V}O(HL'^{4})(OEt)]$ ($\mathbf{I_d^4}$).

Table 2. Cyclic voltammetric results for **1**–**5** and ($\mathbf{I_d^4}$) at 298 K.[a]

Complex	$E^{c}_{1/2}$(V), E_{pc}(V)	ΔE_p (mV)	$E^{a}_{1/2}$ (V)	ΔE_p (mV)
$[Mo_2^{V}O_2L'^{1}_2]$ (**1**)	–0.61, –1.36	372	0.76, 1.14	300, 130
$[Mo_2^{V}O_2L'^{2}_2]$ (**2**)	–0.63, –1.33	340	0.75, 1.11	300, 120
$[Mo_2^{V}O_2L'^{3}_2]$ (**3**)	–0.62, –1.35	365	0.76, 1.13	310, 140
$[Mo_2^{V}O_2L'^{4}_2]$ (**4**)	–0.63, –1.37	370	0.78 , 1.14	310, 110
$[Mo^{VI}O_2L^{5}]$ (**5**)	–0.89, –1.69	270	-	-
$[Mo^{V}O(HL'^{4})(OEt)]$ ($\mathbf{I_d^4}$)	–0.91	286	1.04	250

[a]Solvent: DMF for **1**–**5** and DMSO for $\mathbf{I_d^4}$; Pt working and auxiliary electrodes and SCE as reference electrode and TBAP as supporting electrolyte; scan rate: 50 mV/s. $E^{c}_{1/2} = (E_{pa} + E_{pc})/2$, where E_{pa} and E_{pc} are anodic and cathodic peak potentials vs. SCE, respectively. $\Delta E_P = E_{pa} - E_{pc}$.

Description of X–ray structure of dinuclear Mo(V), [$Mo_2^VO_2L'_2^{1,2,4}$](1, 2 and 4) and mononuclear Mo(VI), [$Mo^{VI}O_2L^5$] (5) complexes. The molecular structure of the dinuclear [$Mo_2^VO_2L'_2^{1,2,4}$] (**1**, **2** and **4**) and mononuclear [$Mo^{VI}O_2L^5$] (**5**) complexes were determined by the single crystal X-ray diffraction technique, and ORTEP representations for the complexes are shown in Figure 5. The relevant bond distances and angles are collected in Tables 3 and 4.

The structures of **1**, **2** and **4** contain dinuclear $[Mo^V_2O_2]^{6+}$ cores with Mo–Mo bonds. The rearranged ligands ($H_3L'^{1,2,4}$) coordinate each molybdenum atom through one phenoxido oxygen, one imino nitrogen and one bridging imido nitrogen in a tridentate chelating manner (formation of [$Mo_2^VO_2L'_2^{1–4}$] (**1–4**) is given in Scheme 2). Disregarding the metal-metal bond, each molybdenum atom exists in a distorted square-pyramidal geometry where the MoN_3O_2 coordination environment comprises of two imido-bridged nitrogen atoms, one imino nitrogen atom, and one phenoxido oxygen atom describing the equatorial plane, and one oxido oxygen as an axial group. Distortion of the square plane is evident from the difference in the Mo–O(1)/O(2), Mo–N(1)/N(3), Mo–N(2), and Mo–N(4) bond lengths as well as the difference in the bond angles at the Mo atom [74.6(7) to 109.4(2)°]. The lengths of the Mo=O, Mo–O, Mo–N_{imino} and Mo–N_{imido} bonds are unexceptional.[1,9e,49a,b,c,54] Both Mo acceptor centers are displaced from the average equatorial plane described by O(1)/O(2)–N(1)/N(3)–N(2)– N(4) towards the axial oxido oxygen atom O(3)/O(4) by about 0.63(1) Å, the distance of O(3)/O(4) from the same plane being about 2.3 Å. Such a displacement of the Mo atom from the equatorial plane towards the apical oxido oxygen atom is also found in the aldehyde oxidoreductase of *Desulfovibrio gigas.*[55] This displacement, naturally, makes each Mo^V acceptor center somewhat inaccessible to the donor approaching from the opposite direction. Hence, it is evident that the discrete [$Mo_2^VO_2L'_2^{1-4}$] molecule has a square-pyramidal structure with the sixth position, *trans* to the oxido oxygen atom O(3)/O(4), vacant. The Mo–N_{imido} bond length is shorter

than the Mo–N_{imine} bond length, indicating that the deprotonated bridging imido-N coordinates more strongly to the metal centre than the imino group. The average bite angle of the tridentate ligands, 79.15°, deviates significantly from 90°, which is the main reason for the structural distortion of complexes **1**, **2** and **4** from the ideal geometry. The Mo(1)–Mo(2) bond distance in **1**, **2** and **4** ranging between 2.64–2.66 Å indicates the formation of a localized metal-metal single bond.[1,3i,3j, 48b,c,56] Here, it is worth mentioning that this is the first structural evidence of metal-metal bonded oxidomolybdenum(V) complexes synthesized from salen type ligands containing aromatic imine group. Earlier there have been reports on molybdenum complexes of similar ligands where molybdenum(VI) oxido[35a,b,c] or peroxido[35d] structures were proposed on the basis of assumptions from spectral data. However, the structures of **1**, **2** and **4** clearly indicate that *in situ* reduction of salophen ligands, containing an aromatic imine moiety, takes place in presence of molybdenum acetylacetonate leading to the formation of dimeric oxidomolybdenum(V) complexes.

The mononuclear dioxidomolybdenum(VI) complex (**5**) shows a distorted octahedral geometry involving NO_3 donors as the basal plane taken up by one tertiary nitrogen N(1), two phenolate oxygen atoms O(1) and O(2), all from the tetradentate ligand $(L^5)^{2-}$, together with a terminal oxido ligand O(3). Another terminal oxido oxygen atom O(4) and one tertiary nitrogen N(2), from the ligand, is attached to the metal atom to fill its two axial sites and form a *trans* O(4)–Mo–N(2) angle of 167.0(2)°. The Mo atom lies 0.315(3) Å out of this mean meridional plane in the direction of O(4) atom. The rather long Mo–N distance 2.28 (8) Å of the tertiary nitrogen N(2), from the ligand, to the sixth coordination position lying *trans* to the oxido-oxygen O(4) may be a consequence of displacement of the Mo atom from the equatorial mean plane towards the apical oxido-oxygen O(4). The Mo–O(3) and Mo–O(4) bond distances of the MoO_2^{2+} group are unexceptional.[38b,47e,52c,57] All these structural features as well as bonds lengths and angles values are in good accordance with similar *cis*-MoO_2L complexes of related N_2O_2 ligands reported earlier.[52c,58]

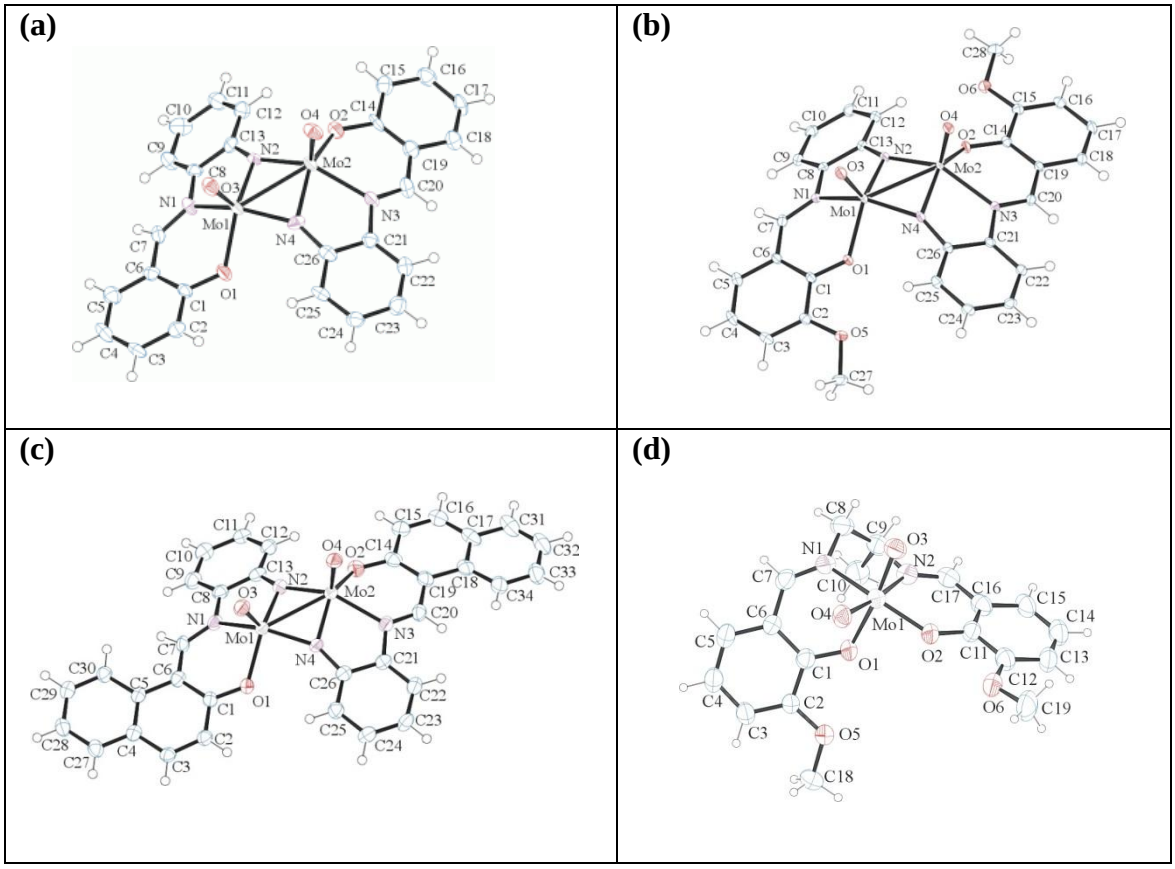

Figure 5. ORTEP representations of compounds (a) $[Mo_2^{V}O_2L'_2{}^{1}]$ (**1**), (b) $[Mo_2^{V}O_2L'_2{}^{2}]$ (**2**), (c) $[Mo_2^{V}O_2L'_2{}^{4}]$ (**4**) and (d) $[Mo^{VI}O_2L^{5}]$ (**5**) with displacement parameters of **1**, **2** and **4** at 50% and **5** at 30% probability.

Table 3. Selected bond distances (Å) and angles (˚) for complexes **1**, **2** and **4**.

Complex	**1**	**2**	**4**
Bond distances (Å)			
Mo1-O1	2.028(4)	2.016(2)	2.034(3)
Mo2-O2	2.020(5)	2.020(2)	2.035(5)
Mo1-O3	1.683(4)	1.693(2)	1.698(4)
Mo2-O4	1.687(5)	1.696(2)	1.703(4)
Mo1-N1	2.170(7)	2.167(2)	2.163(4)
Mo1-N2	1.947(5)	1.961(2)	1.974(4)
Mo2- N2	1.938(5)	1.962(2)	1.979(4)
Mo2- N3	2.175(5)	2.187(2)	2.153(4)
Mo1- N4	1.935(6)	1.948(2)	1.963(4)
Mo2- N4	1.955(5)	1.960(2)	1.966(4)
Mo1-Mo2	2.650(1)	2.656(3)	2.640(6)
Bond angles (°)			
O1-Mo1-N1	83.7(2)	82.7(7)	82.6(1)
O2-Mo2-N3	84.1(2)	82.9(6)	82.6(1)
O3-Mo1-O1	106.9(2)	108.5(7)	109.0(2)
O4-Mo2-O2	106.8(2)	109.2(7)	109.4(2)
N2-Mo1-N1	75.2(2)	75.7(7)	75.0(2)
N4-Mo2-N3	75.4(2)	74.6(7)	75.8(2)
Mo1-N2-Mo2	86.0(2)	85.2(7)	83.8(2)
Mo1-N4-Mo2	85.9(2)	85.6(7)	84.4(2)
N4-Mo1-O1	87.1(2)	85.7(7)	87.7(2)
N2-Mo2-O2	87.6(2)	86.8(7)	86.4(2)
O3-Mo1-Mo2	106.7 (2)	108.9(6)	105.4(1)
O4-Mo2-Mo1	105.6(2)	108.0(5)	105.4(1)

Table 4. Selected bond distances (Å) and angles (˚) for complex **5**.

Complex 5			
Bond distances (Å)		Bond angles (°)	
Mo1-O1	2.101(4)	O1-Mo1-N1	89.4(2)
Mo1-O2	1.918(4)	O2-Mo1-N2	167.0(2)
Mo1-O3	1.689(5)	O5-Mo1-N2	82.3(2)
Mo1-O4	1.701(5)	O4-Mo1-N2	167.0(2)
Mo1-N1	2.133(7)	N1-Mo1-N2	71.9(2)
Mo1-N2	2.279(8)	O1-Mo1-O2	102.9(2)

DNA binding studies. In order to understand the binding of the molybdenum complexes **1**–**5** to CT-DNA, different spectroscopic techniques were used.

Absorption spectroscopic studies. The absorption bands of the complexes **1**–**5** originating in the regions 430–485 and 275–390 nm are attributed to L–Mo(dπ) LMCT and intra-ligand transitions, respectively.[49a] The equilibrium binding constant (K_b) of the complexes to CT-DNA was determined by UV-Vis titration experiments (Table 5 and Figure 6). On addition of CT-DNA to the complex solution, the UV-Vis absorption bands in the region 275–390 nm showed a hypochromic shift for **1**–**5** and an appreciable hyperchromic shift in the LMCT band for complex **5** (Figure 6). Both the hypochromism for **1**–**5** and hyperchromism for **5** indicate the interaction between the oxidomolybdenum complexes and CT-DNA. The hypochromic shift due to the intra-ligand transition for the complexes **1**–**5** was taken to calculate the binding affinity of the complexes with CT-DNA. The observed hypochromicity of molybdenum complexes **1**–**5**, in the intra-ligand transition band may be due to the interaction between the electronic states of the chromophores of the ligands and the DNA bases.[59–61a]

Table 5. DNA binding parameters for **1**–**5**.

Complex	Binding constant (K_b)[a] (M^{-1})	ΔT_m[b] (^oC)
1	2.50×10^4	+1.50
2	9.36×10^3	+1.00
3	8.44×10^3	+1.50
4	3.20×10^4	–2.00
5	9.90×10^4	+1.50

[a] DNA binding constants were determined by the UV-Vis spectral method. [b] Change in the melting temperature of CT-DNA.

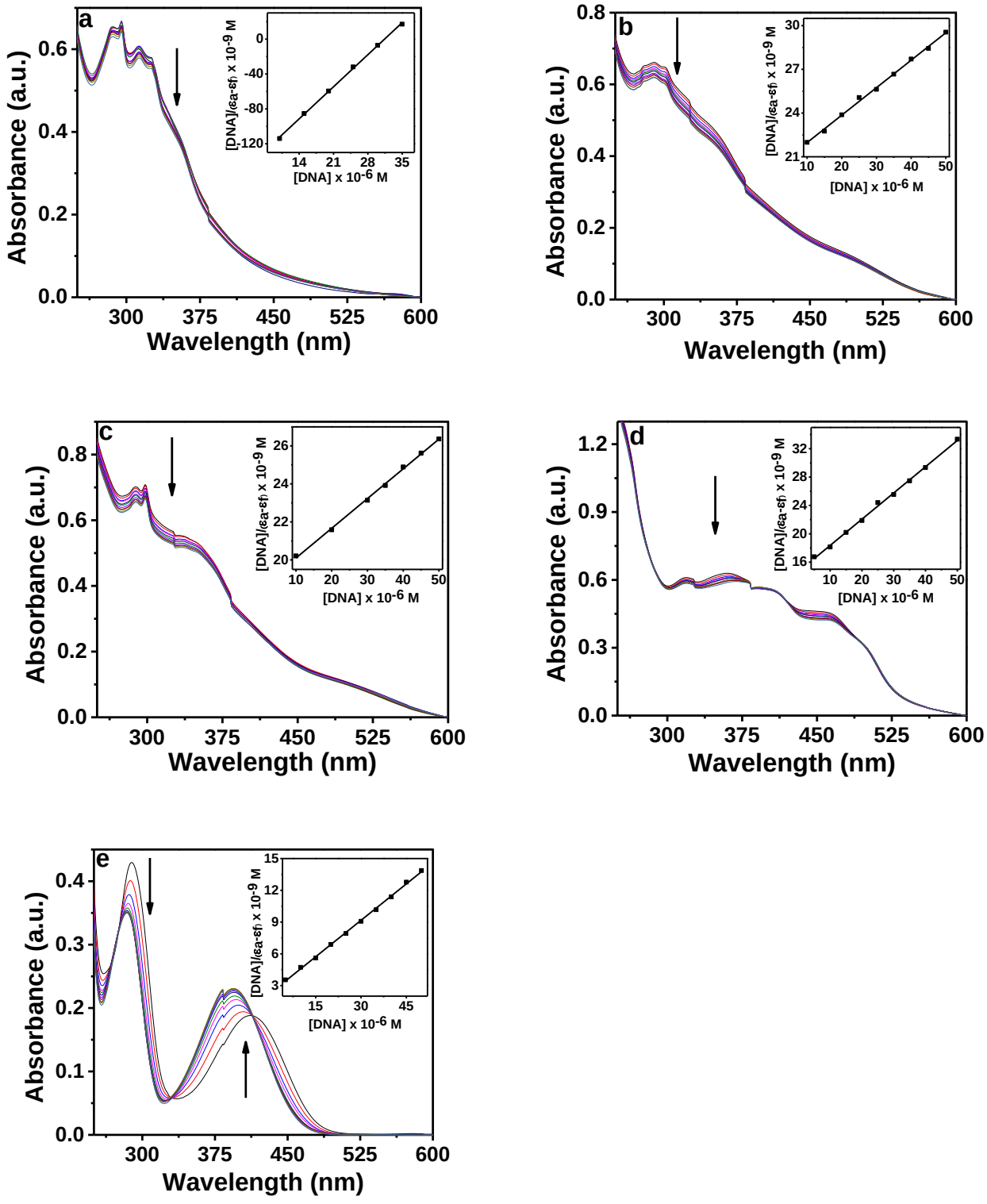

Figure 6. Electronic absorption spectra of **1** (a), **2** (b), **3** (c), **4** (d) and **5** (e) (25 μM) upon the titration of CT-DNA (0–50 μM). The experiments were performed with in 10 mM Tris-HCl buffer (pH 8.0)

containing 1% DMF. Arrow shows the changes in absorbance with respect to an increase in the CT-DNA concentration. The inset shows the linear fit of [DNA]/($\varepsilon_a - \varepsilon_f$) vs [DNA] and the binding constant (K_b) was calculated using Eq. 1.

The binding affinity of the interaction between CT-DNA and each of the molybdenum complexes **1**–**5** is indicated by the binding constant, K_b, which was calculated using Eq. 1. The data reported in Table 5 reveal that the DNA binding strength of the molybdenum complexes are in the order **5 >4 >1 >2 >3**, with the K_b values of **1**–**5** ranging from 9.90×10^4 to 8.44×10^3 M^{-1}. The binding affinity of the ligands to CT-DNA gave values lower than their corresponding molybdenum complexes (Figure S8 and Table S2). The order of the binding affinity can mainly be attributed to the small size of the complexes (especially complex **5**) and incorporation of the electron donating groups attached to the aromatic rings in the ligands.[61b,c] Apart from this, both the phenyl and the napthyl groups in these ligands may also play an important role in the interaction of the complexes with CT-DNA.[61d]

Thermal denaturation studies. In order to investigate the stability of the CT-DNA in presence and absence of the molybdenum complexes **1–5**, DNA melting experiments were performed.[47a] The melting temperature (T_m) of CT-DNA in absence of any complex was ~66 °C, which is in good agreement with our previous finding.[38c-g] Upon interaction with **1**–**3** and **5**, the T_m of CT-DNA increased very slightly (~1.00–1.50 °C), whereas upon interaction with **4**, the same was decreased slightly (~2.0 °C) in Figure 7 and Table 5. The low ΔT_m values for **1**–**3** and **5** indicate that these complexes may bind to CT-DNA through groove binding mode rather than an intercalative mode of binding, which generally gives a large positive ΔT_m value.[62] Complex **4** showed a slight negative ΔT_m value of ~2.00 °C (Table 5 and Figure 7) which may be due to the destabilisation of the DNA double helix by this complex.[63]

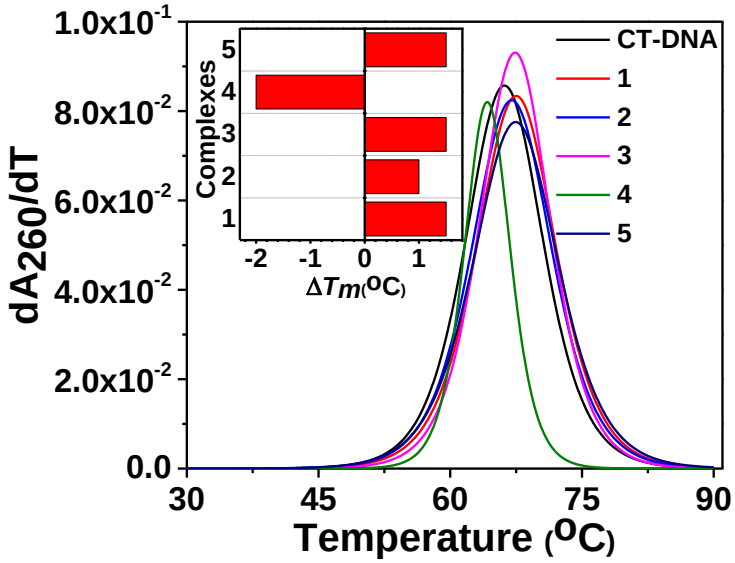

Figure 7. Derivative plot of thermal denaturation of CT-DNA (100 μM) in the absence and presence of **1**–**5** (25 μM) in 10 mM Tris-HCl buffer (pH 8.0) containing 1% DMF. Inset shows the ΔT_m (^{o}C) of the complexes as compared to CT-DNA.

Circular dichroism studies. Circular dichroism (CD) spectroscopy was used in order to study the conformational changes in CT-DNA upon the interaction with complexes.[64] Two conservative CD bands in the UV region are observed for CT-DNA: a positive band at 275 nm which is mainly due to base stacking interaction and a negative band at 245 nm which is due to right-handed helicity.[65a] Groove binding of small molecules show less or no perturbation on the base stacking and helicity bands whereas an intercalation mode can induce intensity changes of both bands, thus modulating the right-handed B-conformation of DNA.[64] The CD spectra of CT-DNA (100 μM) upon the interaction with the oxidomolybdenum complexes showed very slight changes, for the positive band at 275 nm as well as for the negative band at 245 nm (Figure S9) which suggest that the interaction of the oxidomolybdenum complexes **1–5** were groove binding (possibly minor groove binding mode) in nature.

Solution phase fluorescence. The complexes **1–4** exhibited blue fluorescence when exposed to UVA radiation which was readily observed with the naked eyes (Figure 8a-d, inset). Complex **5** did not exhibit any blue fluorescence (Figure 8e, inset). In order to confirm the blue fluorescence properties of the molybdenum complexes, fluorescence emission spectra of the complexes **1–5** were recorded with spectrofluorimeter (Fluromax4P, Horiba Jobin Mayer, USA). All the complexes were excited at 355 nm and the emission spectra were recorded from 370 to 600 nm. The emission maxima of the complexes **1–4** were 418, 434, 436 and 453 nm, respectively (Figure 8 a-d), which lies in the blue region of the visible spectrum. The fluorescence intensities of the complexes decreased in the order **1** > **2** > **3** > **4** (Figure 8 a-d). Complex **5** did not show any fluorescent peak when excited at a wavelength of 355 nm, which was coherent with our previous observation with naked eyes (Figure 8e). Control fluorescence experiments revealed that the ligands have very weak fluorescence as compared to their corresponding molybdenum complexes (Figure S10). Therefore it can be inferred that complexation of the ligands with molybdenum leads to the blue fluorescence characteristics of the complexes **1–4**.

Since, the fluorescence pattern (excitation λ_{max} = 355 nm and emission λ_{max} = 418-453 nm) of all the molybdenum complexes overlaps with the fluorescence characteristics of DAPI (excitation λ_{max} = 358 nm and emission λ_{max} = 455 nm), competitive DNA binding studies by fluorescence measurements using DAPI, could not be performed. In order to assess the major groove and intercalative binding mode, competitive binding experiments were carried out with methyl green (MG) and ethidium bromide (EB), respectively.[38e] But, we did not observe any quenching in the fluorescence of MG and EB bound to CT-DNA (672 nm and 597 nm, respectively) upon the successive addition of the complexes **1**–**5**.[38e] Hence, the complexes don't interact with CT-DNA either by major groove or intercalative mode of binding. In other way, these two competitive binding results hinted towards the

possibility of interaction of these complexes with CT-DNA *via* minor groove binding mode. In fact, thermal denaturation and circular dichroism findings also indicated the similar possibility i.e. the complexes **1**−**5** possibly interact with the CT-DNA by minor groove binding mode.

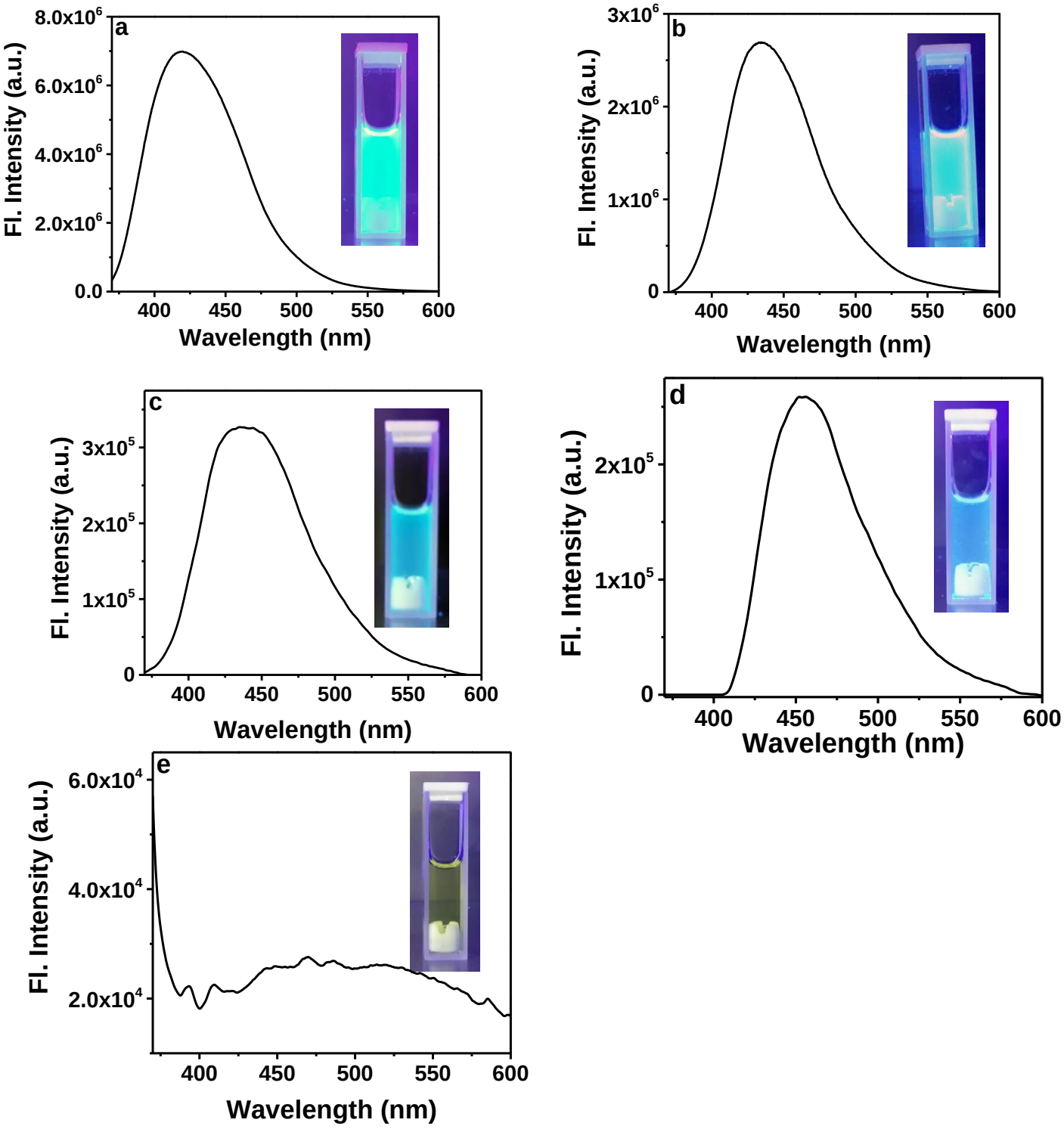

Figure 8. Fluorescence spectra of complexes **1–5** (100 μM) was recorded in the range 370–600 nm at 25°C. The excitation wavelength was 355 nm. Excitation and emission slit width were 5 nm each. Data were recorded at a wavelength resolution of 0.5 nm.

DNA cleavage studies

Chemical-induced DNA cleavage. The chemically induced DNA cleavage activity of the molybdenum complexes **1**–**5** (1–100 μM) was studied using supercoiled pUC19 DNA (300 ng) in 50 mM Tris-HCl buffer (pH 8.0) containing 1% DMF in the dark in the presence of hydrogen peroxide (500 μM) as the oxidising agent. The molybdenum complexes do not exhibit any chemical-induced DNA cleavage activity.

Photo-induced DNA cleavage. To investigate whether the molybdenum complexes possess photo-nuclease activity, a photo-induced DNA cleavage activity assay was performed. The photo-induced DNA nuclease activity of **1**–**5** upon irradiation of UVA light of 350 nm for 3 h in the presence and absence of the molybdenum complexes was studied using supercoiled (SC) pUC19 DNA (300 ng) in 50 mM Tris-HCl buffer (pH 8.0) containing 1% DMF (Figure S11). The decrease in the supercoiled pUC19 DNA (Form I) and subsequent formation of nicked circular DNA (Form II) and linear DNA (Form III) indicated the extent of the DNA cleavage. The percentage of net DNA cleavage by the complexes was estimated using the following equation:

$$\text{Net DNA cleavage } \% = \frac{\text{Form IIs}+2\times\text{Form IIIs}}{\text{Form Is}+\text{Form IIs}+2\times\text{Form IIIs}} - \frac{\text{Form IIc}+2\times\text{Form IIIc}}{\text{Form Ic}+\text{Form IIc}+2\times\text{Form IIIc}} \qquad \text{Eq. 2}$$

The subscripts "s" and "c" refers to the sample and control, respectively.[65a] Since, we did not observe DNA band corresponding to Form III in our photonuclease studies, the concentration of Form III is

put as zero for both 'control' and 'sample'. The DNA cleavage activity of the molybdenum complexes **1**–**5** were carried out in a concentration dependent manner from 1–100 μM. The net DNA cleavage percent by **1**–**5** was plotted with increasing concentration of the molybdenum complexes (Figure 9). Approximately ~1–5% DNA cleavage was observed in the presence of 1 μM of **1**–**3** and **5** whereas at the same concentration **4** exhibited a DNA cleavage of ~37% (Figure 9). The DNA cleavage activity for each of the complexes was saturated at a concentration of 50 μM. At this concentration, the photo-nuclease activity of **1**, **2**, **3**, **4** and **5** was approximately, 17, 26, 36, 93 and 4%, respectively. This indicated that **4** has the most promising photo-nuclease activity among the complex series. Cleavage activity of the complexes (**1**–**5**) varies because of the different functional group present in their ligand moieties.[38c-g] Complex **4** exhibits the highest photonuclease activity which may be due to the presence of extended aromatic ring on the napthyl group[61d] present in the ligand moiety. Apart from this, the presence of the phenyl group and the electron donating groups on the aromatic rings might also influence the DNA cleavage activity of the complexes.[61c] Control experiments revealed that neither DMF (1%) nor the ligand molecules $H_2L^{1\text{-}3}$ and H_2L^5, at a concentration of 50 μM, showed any photo-induced DNA cleavage activity, implying that DMF and the ligands $H_2L^{1\text{-}3}$ and H_2L^5 are cleavage inactive under similar experimental conditions (Figure S12). However, the ligand molecule H_2L^4, at a concentration of 50 μM, showed a DNA cleavage activity of ~20% (Figure S12), which increased significantly upon complexation (~93% at a 50 μM complex concentration) to molybdenum (Figure 9). This indicated that the better activity of complex **4** was due to the presence of naphthyl moiety in the ligand H_2L^4.[66a]

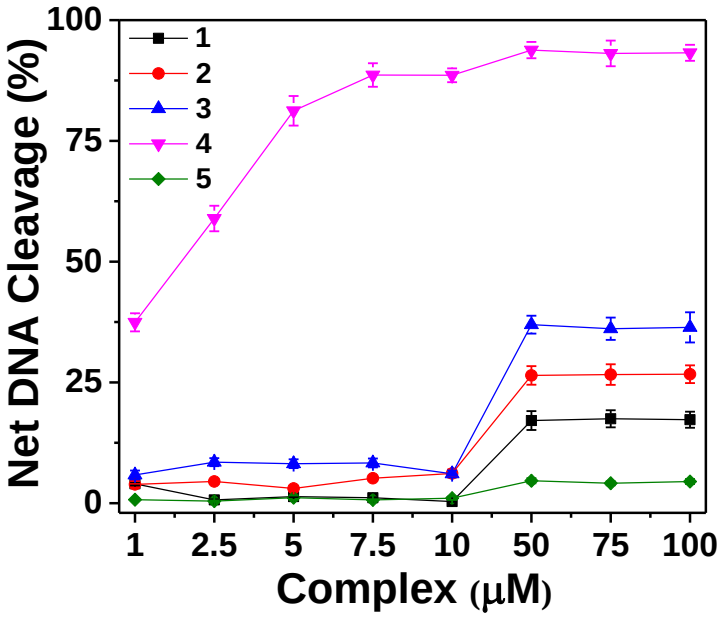

Figure 9. Concentration dependent DNA cleavage of complexes **1**–**5**; 300 ng of SC pUC19 DNA at different concentration of the complexes [1–100 μM in 50 mM Tris-HCl buffer (pH 8.0) containing 1% DMF] was photo-irradiated with UVA at 350 nm for 3 h. The net DNA cleavage percent was calculated using Eq. 2. Each of the data point measured is mean ± standard deviation from triplicate experiments.

In order to understand the mechanistic pathways involved in the photo-cleavage reactions, the photo-induced DNA cleavage activity of **1**–**5** was investigated in the presence of various additives. The DNA cleavage reaction involving molecular oxygen can proceed in two mechanistic pathways: (a) a type-II process involving singlet oxygen species ($^1O_2$), or (b) by a photo-redox pathway involving reactive hydroxyl radicals (·OH).[66b] The addition of NaN_3 (singlet oxygen quencher) and KI (hydroxyl radical quencher) inhibited substantially the DNA cleavage activity of **4** by ~24 and ~54%, respectively (Figure S13 and Figure S14). While, in presence of L-histidine (singlet oxygen quencher) and D-mannitol (hydroxyl radical quencher), the DNA cleavage activity of **4** was restrained by ~14

and ~19%, respectively (Figure S13 and Figure S14). However, no inhibition of DNA cleavage was observed for **1–3** and **5** in the presence of the additives (Figure S13). Therefore, it can be concluded that **4** exhibits photo-induced DNA cleavage activity probably via both singlet oxygen and hydroxyl radical pathways, while the mechanistic pathways involved in the photo-induced DNA cleavage by **1–3** and **5** cannot be distinctly ascertained.

The above results of the DNA interaction studies of the synthesised molybdenum complexes **1–5** are in accordance with previous reports of DNA binding/cleavage studies of related oxidomolybdenum(VI)[67a-d] and those of other transition metal[67e-h] salen complexes. However, the DNA cleavage activity of complex **4** (~93% at a 50 μM complex concentration) is exceptionally better than the previous reports.

Cytotoxicity Studies

MTT assay. The antiproliferative efficacy of **1**–**5** was assayed by determining the viability of MCF-7 (human breast adenocarcinoma), HCT-15 (colon cancer) cells using the MTT assay. The ligands, $H_2L^{1–5}$ and $MoO_2(acac)_2$ gave high IC_{50} values (>200 μM), whereas **1**–**5** gave values in the range 28.52–11.13 μM in MCF-7 cells and between 76.30–32.20 μM in HCT-15 cells (Table 6). In contrast, cisplatin,[68a,b] a commonly used chemotherapeutic drug is comparatively effective in MCF-7 and HCT-15 cells with an IC_{50} value of 7.8 and 12.20 μM under similar experimental conditions. The significant decrease in the inhibitory ability of the ligands as well as their lower binding affinity to CT-DNA compared to their metal complexes clearly indicates that incorporation of molybdenum has a marked effect on cytotoxicity. A possible explanation is that the polarity of the ligand and the central metal ion are reduced by coordination through the charge equilibration, which favors permeation of the complexes through the lipid layer of the cell membrane.[68c,69] The results of DNA

binding/cleavage ability for the ligands have been considered and are consistent with the observation that metal complexes can exhibit greater biological activities than the free ligands.[70]

The cytotoxic activities of the complex series **1**–**5** can be judged from their IC_{50} values (Table 6), with their dose dependency illustrated in Figure 10 and 11. The IC_{50} values of **1**–**5** could be obtained only after 48 h of treatment in MCF-7 and HCT-15 cells. A representative percentage of cell viability of MCF-7 cells after 24 h of treatment with increasing concentrations (5, 10, 25 and 50 μM) of molybdenum complexes (**1**–**5**) and $MoO_2(acac)_2$ is shown in Figure S15.

IC_{50} values of the complexes **1**, **4** and **2** ranges between 11.13–13.25 μM in case of MCF-7 and in case of HCT-15 it ranges between 32.20 −54.92 μM, while **3** and **5** have IC_{50} value in the range 27.31–28.52 μM in case of MCF-7 and between 55.61−76.30 in HCT-15 cells. Since, the variation in the IC_{50} values obtained for complexes **1**, **4** and **2** is distinctly different from that of **3** and **5**, these complexes can be combined into two groups i.e. 'Group 1' corresponding to the complexes with higher cytotoxicity (**1**, **4** and **2**) and 'Group 2' corresponding to the complexes with lower cytotoxicity (**3** and **5**). The cytotoxicity order of the complexes neither matches completely with the DNA binding order nor the photonuclease activity order. However, 'Group 1' complexes with higher cytotoxicity do exhibit comparatively higher photonuclease activity than 'Group 2' complexes which have lower cytotoxicity. The variation in results of cytotoxicity of the complexes may be affected by the various functional groups in the salen ligands. The presence of electron withdrawing Br group in complex **3** leads to an increase in the IC_{50} (less cytotoxicity),[18] while complex **1** which has no substituents on the ligand fragment, and complex **2** which contains an electron releasing –OMe group, exhibits lower IC_{50} (higher cytotoxicity).[18] The considerable efficacy of **4** in MCF-7 cells, as also inferenced from DNA binding/cleavage studies, maybe due to the presence of the naphthyl group in the ligand moiety.[66a] Also, the introduction of aromatic diimine bridges in the salen complexes (**1**, **2** and **4**)

increases their cytotoxicity, as evident from the higher IC_{50} value of complex **5** (less cytotoxicity) which contains an aliphatic diimine bridge.[22c]

The same MTT assay was also performed on noncancerous human keratinocytes HaCaT cell line in order to determine the selectivity of action between healthy and cancerous cells. The very high IC_{50} values of **1**–**5** (96–477.26 μM, Table 6) and their dose dependency (Figure S16) in HaCaT cells indicated that the compounds exhibited no substantial cytoxicity to normal keratinocytes.

In the recent past, some oxidomolybdenum(VI) complexes have been reported to have significant cytotoxic activities against various human cancer cell lines including HL-60 and K562 (leukemia), A-549 (lung cancer), HeLa (cervical carcinoma) and MCF-7 (breast carcinoma).[24,34,67b,71] Salen complexes of some transition metals have also been reported to show appreciable cytotoxic activities against human cancer cell lines.[22a,22c,72] In few cases the results of the above studies are in accordance with the synthesized molybdenum complexes **1**–**5**, while in some cases they exhibit better cytotoxicity than **1**–**5** in terms of IC_{50} values.

Table 6. Cytotoxicity of **1**–**5** as measured by MTT assay in MCF-7, HCT-15 and HaCaT cells.

Complex	MCF-7 IC_{50} values (μM) 48 h	HCT-15 IC_{50} values (μM) 48 h	HaCaT IC_{50} values (μM) 48 h
1	11.13 ± 0.65	32.20 ± 0.92	200.74 ± 0.12
2	13.25 ± 1.32	52.54 ± 2.68	179.47 ± 1.02
3	28.52 ± 2.65	76.30 ± 1.84	477.26 ± 2.36
4	12.43 ± 0.94	54.92 ± 1.06	370.13 ± 0.51
5	27.31 ± 1.83	55.61 ± 0.65	96.00 ± 0.09

*Values are mean ± SD, n=3

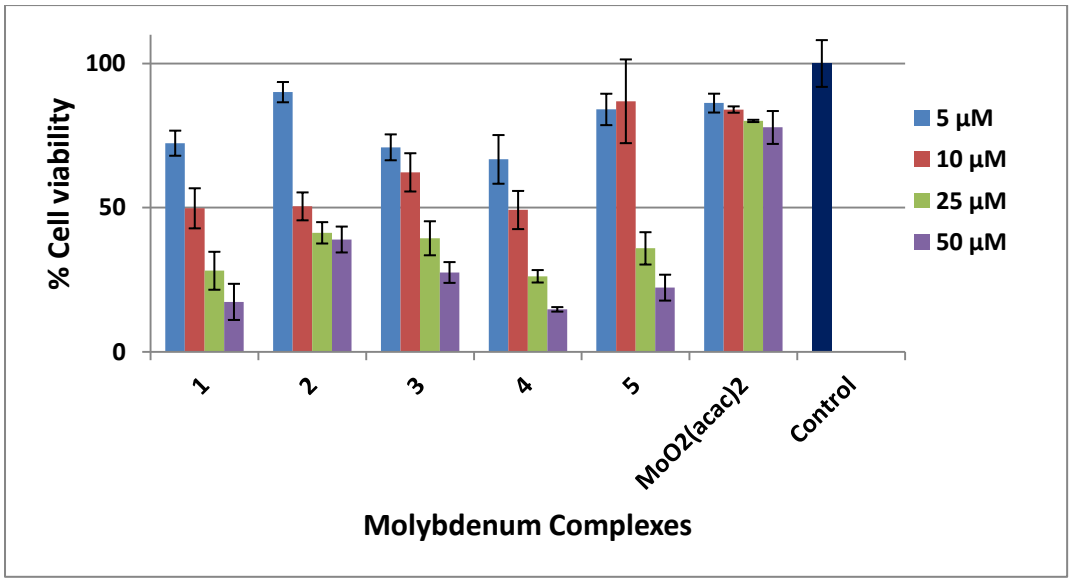

Figure 10. Effect of **1**–**5** on cell viability and growth: MCF-7 cells were treated with different concentrations of the test compound for 48 h and then cell viability was measured by MTT assay. Data reported as the mean ± SD for n = 3.

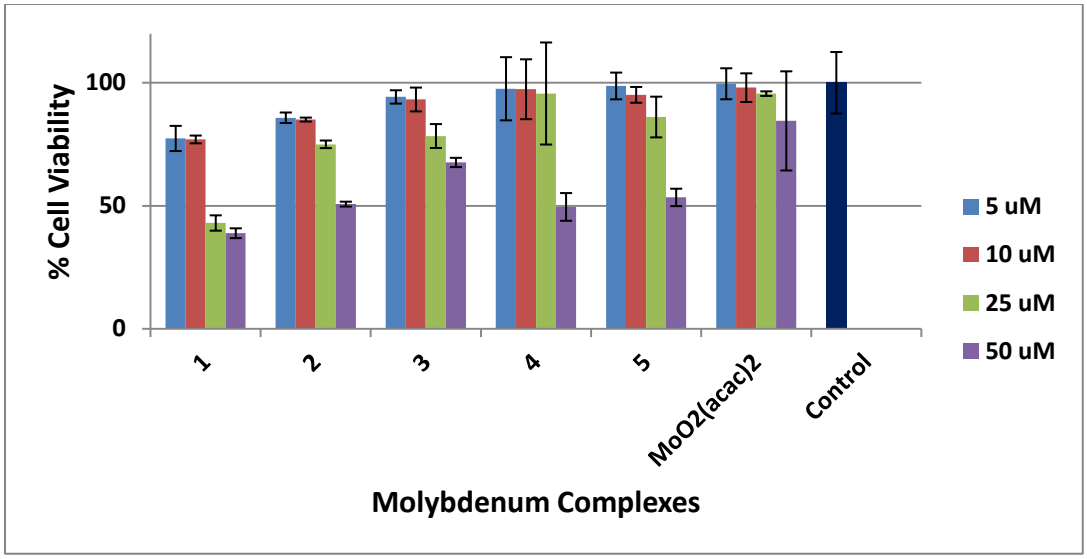

Figure 11. Effect of **1**–**5** on cell viability and growth: HCT-15 cells were treated with different concentrations of the test compound for 48 h and then cell viability was measured by MTT assay. Data reported as the mean ± SD for n =3

Nuclear Morphological Studies

Investigation of apoptotic potential of compounds is usually performed by DAPI staining experiments.[38c-g] However, it was found that the synthesized molybdenum complexes, **1**–**4** themselves exhibited fluorescence emission at the same wavelengths as DAPI (blue region). Hence, the use of DAPI as staining agent was inappropriate in the present situation and therefore it was replaced by Propidium Iodide, which exhibited red fluorescence, to examine the effect of the test complexes on nuclear morphology of MCF-7 cells. The density of the PI stained nuclei was used to check the live cells in different treatment groups. Figure 12 and Figure 13 show images taken after PI staining in red fluorescence at different concentrations of **2** respectively on MCF-7 and HCT-15 cells respectively. Figures S17 and S18 show images taken after PI staining of **1**, **3**–**5** on MCF-7 and HCT-15 cells respectively. It can be seen from the figures that the number of PI stained nuclei were reduced in

treated wells with increasing concentrations of the complexes indicating the dose dependent cell death.[73,74] Figure 12 (b) and Figure 13(b) show the grey scale images at 48 hrs after the treatment with increasing concentrations of the complexes on MCF-7 and HCT-15 cells. The distinct nuclear condensation and fragmentation (indicated by arrows) were seen in treated cells (Figure 12 and 13) compared to control cells (Figure S17(A) and S18(A)).

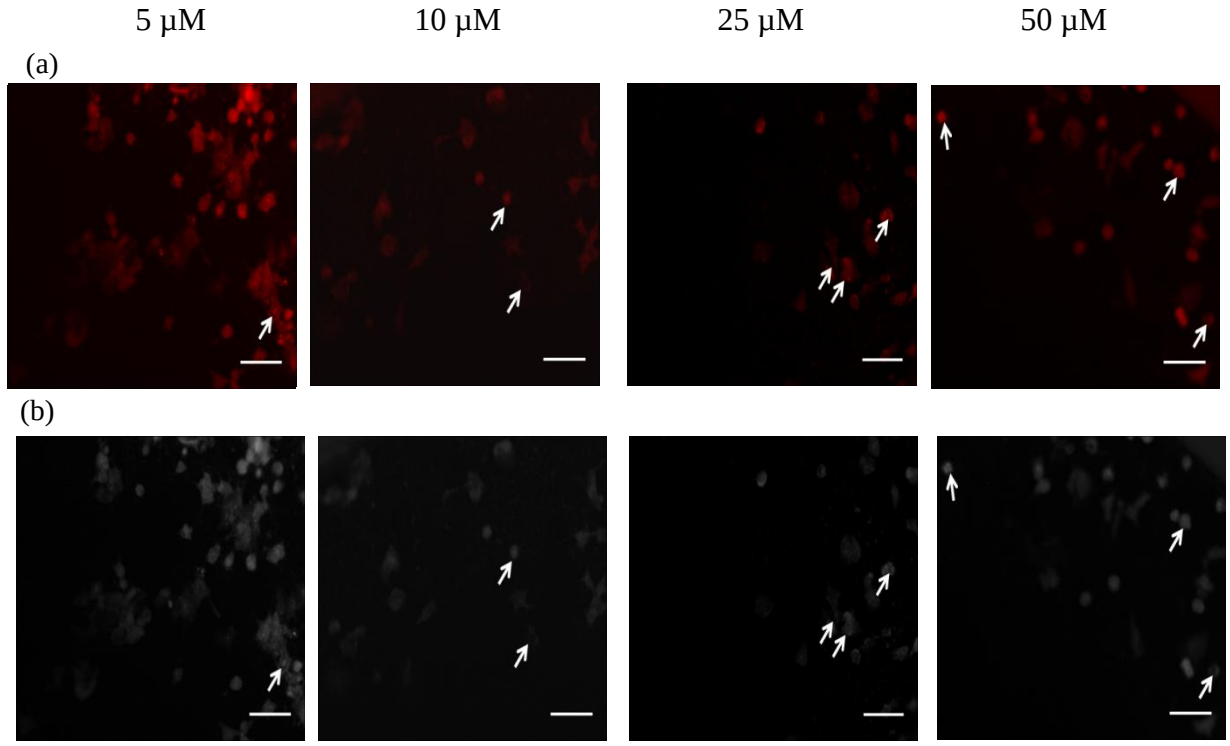

Figure 12. Effect of treatment of complexes on the nuclear morphology of cells. The morphological changes in nuclei of MCF-7 cells from control and treated groups were washed twice with PBS (pH 7.4) and fixed after incubation for 15 min with 3.7 % of formaldehyde. The cells were then washed twice with PBS and treated with 0.2% triton-X 100 in PBS for 30 seconds. Further the cells were washed twice with PBS and PI solution (10 µg/mL) was added and kept for 15 min in dark. Finally the cells were washed twice with PBS and imaged under fluorescence microscope (FLoid, Life technologies). Arrows indicate the morphological changes in nuclei of MCF–7 cells observed on applying increasing concentrations (5, 10, 25 and 50 µM) of **2** in comparison to control. The scale bar corresponds to 100 µm.

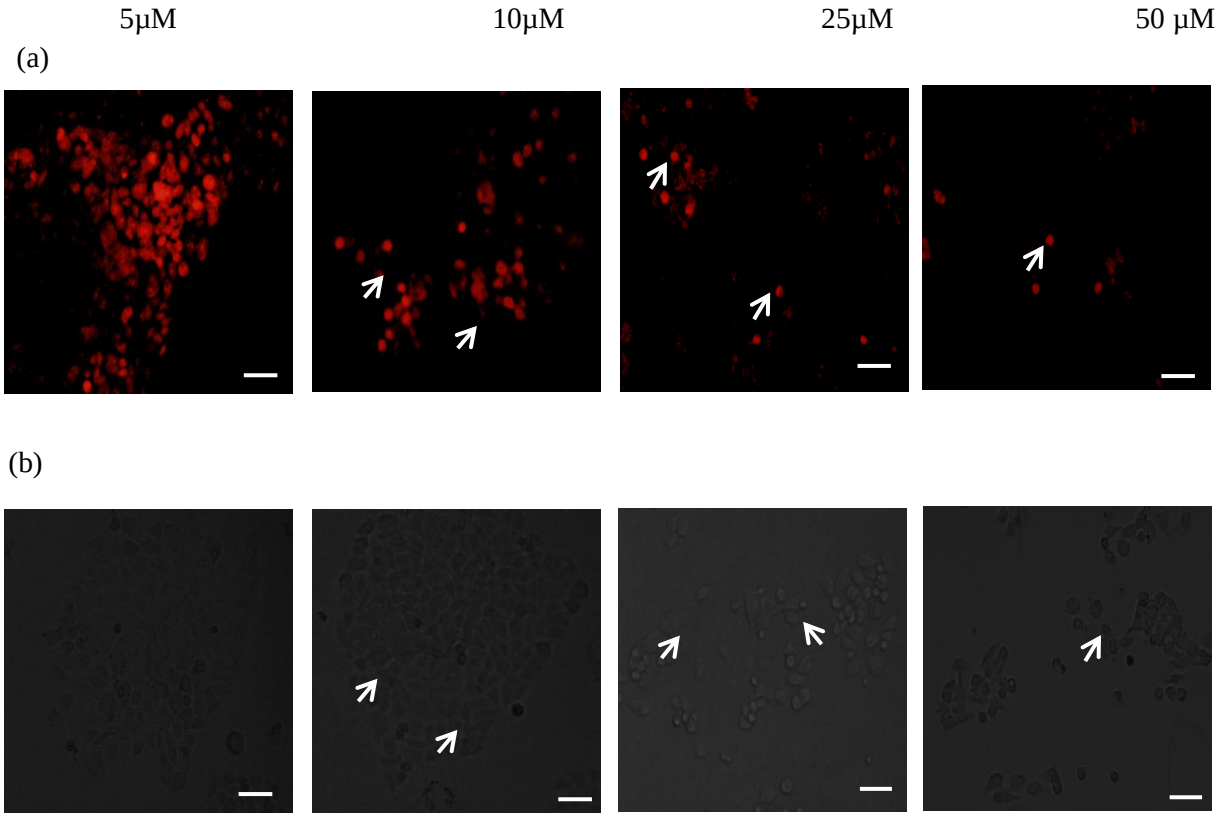

Figure 13. Effect of treatment of complexes on the nuclear morphology of cells. The morphological changes in nuclei of HCT-15 cells from control and treated groups were washed twice with PBS (pH 7.4) and fixed after incubation for 15 min with 3.7 % of formaldehyde. The cells were then washed twice with PBS and treated with 0.2% triton-X 100 in PBS for 30 seconds. Further the cells were washed twice with PBS and PI solution (10 μg/mL) was added and kept for 15 min in dark. Finally the cells were washed twice with PBS and imaged under fluorescence microscope (FLoid, Life technologies). Arrows indicate the morphological changes in nuclei of HCT-15 cells observed on applying increasing concentrations (5, 10, 25 and 50 μM) of **2** in comparison to control. The scale bar corresponds to 50 μm.

CONCLUSIONS

Five salen type ligands from an aromatic diamine, *o*-phenylenediamine ($H_2L^{1\text{-}4}$) and an aliphatic diamine, 1,2-diaminopropane (H_2L^5) were synthesized. $H_2L^{1\text{-}4}$, furnished dimeric bis-μ-imido bridged oxidomolybdenum(V) complexes $[Mo_2^{V}O_2L'_2{}^{1\text{-}4}]$ (**1**–**4**), where $L'^{1\text{-}4}$ indicates the rearranged form of the ligands $H_2L^{1\text{-}4}$, *via* an interesting mechanistic pathway which involves the formation of rare monomeric molybdenum(V) intermediate $[Mo^{V}O(HL'^{1-4})(OEt)]$ ($\mathbf{I_d^{1-4}}$) by the molybdenum assisted hydrolysis of the imine bond and subsequent −C=N bond cleavage of the salophens. The deprotonation and dimerization of Mo(V) intermediates finally resulted in the formation of two imido bridges between the Mo(V) centers containing a metal-metal bond. One of the molybdenum(V) intermediates $[Mo^{V}O(HL'^{4})(OEt)]$ ($\mathbf{I_d^4}$) was isolated in the solid state and characterized by spectral (IR, UV-Vis, EPR) and ESI-MS studies. In case of H_2L^5, no such imine hydrolysis or −C=N bond cleavage in the ligand took place and a monomeric dioxidomolybdenum(VI) complex $[Mo^{VI}O_2L^5]$ (**5**) was furnished. The structures of dimeric metal-metal bonded oxidomolybdenum(V) complexes synthesized from salen type ligands containing aromatic imines were established for the first time through X-Ray crystallography and the mechanistic pathway of their formation was also explained. The disappearance of EPR signals in the Mo(V) intermediate $\mathbf{I_d^4}$ after 30 min also proved the formation of corresponding diamagnetic dimeric bis-μ-imido bridged oxidomolybdenum(V) complexes, where antiferromagnetic coupling[48a] occurs between the two Mo(V) centres. Comparison with several other transition metal complexes of similar ligand systems,[41] where no such ligand transformation takes place, proved that the hydrolysis and −C=N bond cleavage of salophen ligands was Mo assisted.

In vitro biological studies reveal that **1**–**5** show considerable DNA binding propensity. The CD and thermal melting studies revealed that the complexes interact with CT-DNA in a manner consistent

with groove binding mode, with binding constants ranging from 10^3–10^4 M^{-1}. All complexes exhibited good photo-induced cleavage of pUC19 supercoiled plasmid DNA with **4** giving the most promising photo-induced DNA cleavage activity of ~93%. The results from the mechanistic study suggested that the photolytic DNA cleavage of **4** proceeded *via* both singlet oxygen and hydroxyl radical pathways while the mechanistic pathways involved in the photo-induced DNA cleavage by **1-3** and **5** could not be distinctly ascertained. Also, results of antiproliferative activities of the synthesised complexes suggested that they are significantly cytotoxic towards MCF-7 and HCT-15 cell lines. The complexes containing the aromatic diimine moiety (**1**, **2** and **4**) were found to be more cytotoxic than the complex containing the aliphatic diimine (**5**). The presence of electron withdrawing Br group in **3** lowered its cytotoxicity. The better activity of **4** may be attributed to the presence of the naphthyl moiety in the ligand system. Also, **1**–**5** did not exhibit significant cytoxicity to HaCaT cells (normal keratinocytes). The results reported herein will encourage further work on oxidomolybdenum complexes for the development of metal-based agents for anticancer studies.

SUPPORTING INFORMATION

^{1}H NMR of $H_2L^{1\text{-}5}$ and $[Mo_2^{V}O_2L'_2{}^{1\text{-}4}]$ (**1**-**4**) and $[Mo^{VI}O_2L^5]$ (**5**) (Table S1), Binding constant (K_b) values for the "CT-DNA-ligand" interactions (Table S2), Absorption spectral traces of the complexes up to 72 h **1** (a), **2** (b), **3** (c), **4** (d) and **5** (e) (25 μM each) in 10 mM Tris-HCl buffer (pH 8.0) containing 1% DMF. (Figure S1(A)), ^{1}H NMR spectra of complex **2** in DMSO-d_6 after 0 h (a), ^{1}H NMR spectra of complex **2** in DMSO-d_6 after 72 h (b) and after heating (120 °C) the solution and (c) (Figure S1(B)), UV-vis spectra of the complexes (**1**–**5**) (5 μM) in [A] DMSO and [B] water (Fig. S1.(C)), FTIR spectra of $[Mo^{V}O(HL'^{4})(OEt)]$ ($\mathbf{I_d^4}$) (Figure S2(a)) and $[Mo_2^{V}O_2L'_2{}^{4}]$ (**4**) (Figure S2(b)), Absorbance spectrum of $[Mo^{V}O(HL'^{4})(OEt)]$ ($\mathbf{I_d^4}$) (Figure S3(a)) and $[Mo_2^{V}O_2L'_2{}^{4}{}_2]$ (**4**) (Figure S3(b)), ^{1}H NMR spectra of H_2L^2 (Figure S4(a)) and $[Mo_2^{V}O_2L'_2{}^{2}]$ (**2**) (Figure S4(b)), ^{1}H NMR of $[Mo_2^{V}O_2L'_2{}^{3}]$ (**3**) (Figure S5), ^{13}C NMR of $[Mo_2^{V}O_2L'_2{}^{3}]$ (**3**) (Figure S6), ESI-MS spectrum of $[Mo_2^{V}O_2L'_2{}^{3}]$ (**3**) (Figure S7), Electronic absorption spectra for H_2L^1 (a) H_2L^2 (b), H_2L^3 (c) H_2L^4 (d) and H_2L^5 (e) (25 μM each) upon the titration of CT-DNA (0 – 250 μM) in 10 mM Tris-HCl buffer (pH 8.0) containing 1% DMF (Figure S8), Circular dichroism spectra of CT-DNA (100 μM) in the presence and absence of complexes **1**–**5** (25 μM each) (Figure S9), Fluorescence spectra of complexes $H_2L^{1\text{-}5}$ (Figure S10), Gel diagram showing concentration dependent DNA cleavage by **1**–**5** (Figure S11), Gel diagram showing the effect of DMF (1%) and ligands on the photo-induced cleavage of SC pUC19 DNA (Figure S12), DNA cleavage of SC pUC19 DNA by **1**–**5** in presence of various additives in 50 mM Tris-HCl buffer (pH 8.0) containing 1% DMF (Figure S13), Gel diagram depicting cleavage of SC pUC19 DNA by **1**–**5** in presence of various additives (Figure S14), Effect of **1**–**5** on cell viability and growth of MCF-7 cells after 24 hours (Figure S15), Effect of **1**–**5** on cell viability and growth of HaCaT cells after 48 hours (Figure S16), Changes in nuclei morphology with respect to treatment concentration of molybdenum complexes (**1**, **3**, **4** and **5**) in comparison to control

in MCF-7 cells (Figure S17), Changes in nuclei morphology with respect to treatment concentration of molybdenum complexes (**1**, **3**, **4** and **5**) in comparison to control in HCT-15 cells (Figure S18).

Supporting Information is available free of charge via the Internet at http://pubs.acs.org.

The crystallographic data for the structural analysis of **1**, **2**, **4** and **5** have been deposited with the Cambridge Crystallographic Data Centre, CCDC No. for **1** is 1491690, for **2** is 1491692, for **4** is 1491691, and **5** is 1491689. A copy of this information may be obtained free of charge from the CCDC, 12 Union Road, Cambridge CB2 1EZ, UK (Tel.: +44 (0) 1223 762911;

E-mail: deposit@ccdc.cam.ac.uk.

AUTHOR INFORMATION

Corresponding Authors

*E-mail: rupamdinda@nitrkl.ac.in (R. Dinda)

Author Contributions

The manuscript was written through contributions of all authors. All authors have given approval to the final version of the manuscript.

Notes

The authors declare no competing financial interest.

ACKNOWLEDGEMENTS

Funding for this research was provided by Council of Scientific and Industrial Research, Government of India (Grant No. 01(2735)/13/EMR-II) and DBT, Govt. of India [Grant No. 6241 P112/RGCB/PMD/DBT/RPDA/2015].

REFERENCES

(1) Modec, B.; Brenčič J. V.; Koller, J. A Series of Molybdenum(V) Complexes with the Oxalato Ligand Engaged in Different Binding Roles −An Unusual Staggered Conformation of the μ_4-Oxalate in $[\{Mo_2O^4(\eta^2\text{-}C_2O_4)_2\}2(\mu_4\text{-}C_2O_4)]^{6-}$. *Eur. J. Inorg. Chem*. **2004**, 1611−1620.

(2) Modec, B.; Brenčič, J. V. From Small $\{Mo_2O_4\}^{2+}$ Aggregates to Infinite Solids. *J. Cluster Sci*. **2002**, *13*, 279–302.

(3) (a) Delbaere, L. T. J.; Prout, C. K. The X-ray Crystal and Molecular Structure of a Molybdenum(V)-L-Histidine Complex Mo_2O_4(L-histidine)$_2$,3H_2O. *J. Chem. Soc., D Chem. Commun.* **1971**, 162−162. (b) Beaver, J. A.; Drew, M. G. B. Crystal and Molecular Structure of Tetrachloro-di-μ_3-oxo-tetra-μ-prop-oxo-tetraoxodipropoxotetramolybdenum(2*MO–MO*). *J. Chem. Soc., Dalton Trans*. **1973**, 1376–1380. (c) Modec, B.; Brenčič, J. V.; Golič, L.; Giester, G. Oxomolybdenum Coordination Compounds with Pyridine. Syntheses and Structures of $[Mo_4O_8(OCH_3)2Cl_2L_4]\cdot 2L$ (L=Py, 4-MePy), $[Mo_4O_8(OCH_3)_4(4\text{-}MePy)_4]$, $[Mo_6O_{12}(OCH_3)6Py_4]$ and $[Mo_{10}O_2 6Py_8]\cdot 7Py$. *Inorg. Chim. Acta* **2000,** *307*, 33–41. (d) Zhou, Z.; Xu, Q; Lin, J; Ng, S. -W. pH Dependent Formations of Dinuclear Molybdenum(V) and Incomplete Cubane Molybdenum(IV) Complexes with Nitrilotriacetate. *Inorg. Chem. Commun*. **2007**, *10*, 1461–1464. (e) Modec, B.; Brenčič, J. V. Novel Hydrogenmaleato Molybdenum(V) Complexes Based on a Dinuclear Metal–Metal Bonded Unit: Syntheses and Structural Characterization of $(PyH)_3[Mo_2O_4Cl_4(OOCCH{=}CHCOOH)]$ and $(PyH)_3[Mo_2O_4Br_4(OOCCH{=}CHCOOH)]$ CH_3CN. *Inorg. Chem. Commun.* **2004**, *7*, 516–520. (f) Zhou, Z.-H.; Deng, Y.-F.; Cao, Z.-X.; Zhang, R.-H.; Chow, Y. L. Dimeric Dioxomolybdenum(VI) and Oxomolybdenum(V) Complexes with Citrate at Very Low pH and Neutral Conditions. *Inorg. Chem.* **2005**, *44*, 6912–6914. (g) Modec, B.; Dolenc, D. Molybdenum(V) Complexes with Formate: Geometric Isomerism of the

$[Mo_2O_4Cl_2(Py)_2(HCOO)]^-$ Ion. *J. Mol. Struct*. **2013**, *1051*, 354–360. (h) Shibahara, T.; Ogasahara, S.; Sakane, G. catena-Poly[[di-aqua-zinc(II)]-μ-L-cystein-ato(2−)-κ^4S:S,N,O-[di-μ-sulfido-bis[oxido-molybdate(V)](Mo—Mo)]-μ-L-cysteinato(2−)-κ^4S,N,O:S]. *Acta Crystallogr. Sect. E*. **2008**, *64*, m605–m606; (i) Wu, P.-F.; Li, D. -S.; Meng, X. -G.; Zhong, X.-L.; Jiang, C.; Zhu, Y.-L.; Wei, Y.-G. Di-μ-oxo-bis-[(histidinato-κ^3N,N,O)oxomolybdenum(V)] Trihydrate. *Acta Crystallogr. Sect. E*. **2005**, *61*, m1553–m1555. (j) Tašner, M.; Prugovečki, B.; Soldin, Z.; Prugovečki, S.; Rukavina, L.; Matković -Čalogović, D. Synthesis and Characterization of Oxomolybdenum(V) Dinuclear Complexes with *β*-Alanine, $_L$-Serine and $_{DL}$-Isoleucine. *Polyhedron*, 2013, *52*, 268–275. (k) Meienberger, M. D.; Morgenstern, B.; Stucky , S.; Hegetschweiler, K. Polymerization of Mo^V: Synthesis and Characterization of a Dinuclear Mo^V and a Hexanuclear Mixed-Valence Mo^V/Mo^{VI} Complex. *Eur. J. Inorg. Chem.* **2008**, 129–137. (l) Cindrić, M.; Pavlović, G.; Vrdoljak, V.; Kamenar, B. Hexanuclear Complexes of Molybdenum(V) Containing $[Mo_6O_{12}(OCH_3)_4(acac)_3]^-$ Anion. *Polyhedron* **2000**, *19*, 1471–1478. (m) Majumdar, M.; Patra, S. K.; Bera, J. K. Oxidative Route to Polyoxomolybdates from Quadruply Bonded $[Mo^{II}{\equiv}Mo^{II}]$ Precursor: Structural Characterization of a Tetranuclear Cluster $[Mo_4Cl_5O_8(pyNP)_2]$ (pyNP = (2-(2-pyridyl)1,8-naphthyridine)). *Polyhedron* **2007**, *26*, 1597–1602. (n) Sreehari, S.; Luck, R. L. *J. Cluster Sci*. **2010**, *21*, 525–541.

(4) (a) Hsieh, T.-C.; Gebreyes, K.; Zubieta, J. Studies of Molybdenum Thiolato-Complexes. The Chemical Characterization and the Crystal and Molecular Structures of Two Sulphido-Bridged Mo^V Dimers, $[PhCH_2PPh_3]_2[Mo_2O_2S_2(SC_2H_4S)_2]$ and $[HNEt_3]_2[Mo_2S_4(SC_2H_4S)_2]$. *Transition Met. Chem*. **1985**, *10*, 81–84. (b) Martinez, M.; Ooi, B.-L.; Sykes, A. G. Reaction Paths in the Formation of Triangular and Cuboidal Molybdenum/Sulfur Cluster Complexes as Aqua Ions by Reduction of Molybdenum(V) Dimers. *J. Am. Chem. Soc*. **1987**, *109*, 4615–4619. (c) Koffi-Sokpa, E. I.; Calfee, D. T.; Allred, B. R. T.; Davis, J. L.; Haub, E. K.; Rich, A. K.; Porter, R. A.; Mashuta,

M. S.; Richardson, J. F.; Noble, M. E. Activation of Ligand Reactivity: Thiolate C−S and Dithiophosphate Ester C−O Heterolyses within a Dimolybdenum(V) System. *Inorg. Chem.* **1999**, *38*, 802–813. (d) Cindrić, M.; -Čalogović, D. M.; Vrdoljak, V.; Kamenar, B. Synthesis and Characterization of a Series of New Thiocarboxylate Complexes of Molybdenum(V). *Inorg. Chim. Acta* **1999**, *284*, 223–228. (e) Yoshida, R.; Ogasahara, S.; Akashi, H.; Shibahara, T. Crystal Structural Diversity of Sulfur-Bridged Cysteinato Dimolybdenum(V) Complexes: The Influence of Counter Metal Cations. *Inorg. Chim. Acta* **2012**, *383*, 157–163. (f) Xu, J.-Q.; Zhou, X.-H.; Zhou, L.-M.; Wang, T.-G.; Huang, X.-Y.; Averill, B. A. The First Binuclear Mo–S Cluster Compound Containing Citrate Ligands, $K_5(NH_4)[Mo_2O_2(\mu\text{-}S)_2(C_6H_4O_7)_2]\cdot CH_3OH\cdot 5H_2O$, Characterized by X-ray Single Crystal Structure Determination. *Inorg. Chim. Acta* **1999**, *285*, 152–154.

(5) (a) Chakrahari, K. K. V.; Dhayal, R. S.; Ghosh, S. Synthesis and characterization of binuclear μ-oxo and μ-telluro molybdenum(V) complexes, $[Cp^*Mo(O)(\mu\text{-}Te)]_2$. *Polyhedron* **2011**, *30*, 1048–1054. (b) Sattler, A.; Parkin, G. Trinuclear, Tetranuclear and Octanuclear Chalcogenido Clusters of Molybdenum and Tungsten Supported by Trimethylphosphine Ligands. *Polyhedron* **2014**, *84*, 74–86.

(6) Bortoluzzi, M.; Hayatifar, M.; Marchetti, F.; Pampaloni, G.; Zacchini, S. Synthesis of Di- and Tetranuclear Oxido-Molybdenum(V) Complexes Containing p-Toluenesulfonates as Ligands: a Joint Spectroscopic, Crystallographic and Computational Study. *Dalton Trans.* **2014**, *43*, 10157–10163.

(7) Bazhenova, T. A.; Lyssenko, K. A.; Kuznetsov, D. A.; Kovaleva, N. V.; Manakin, Y. V.; Savinykh, T. A.; Shestakov, A. F. Methanolysis of $MoCl_5$ in the Presence of Different Alkaline Agents; Molecular Structures of the Polynuclear Molybdenum(V) Methoxides and Electron Charge Density Distribution From X-ray Diffraction Study of the New K–Mo Cluster. *Polyhedron* 2014, *76*, 108–116.

(8) (a) Spivack, B.; Dori, Z. Structural Aspects of Molybdenum(IV), Molybdenum(V) and Molybdenum(VI) Complexes. *Coord. Chem. Rev*. **1975**, *17*, 99–136. (b) Chae, H. K.; Klemperer, W. G.; Paez-Loyo, D. E.; Day, V. W.; Eberspacher, T. A. Synthesis and Structure of a High Nuclearity Oxomolybdenum(V) Complex, $[(C_5Me_5Rh^{III})8(Mo^{V}_{12}O_{36})(Mo^{VI}O_4)]^{2+}$. *Inorg. Chem.* **1992**, *31*, 3187–3189. (c) Chae, H.K.; Klemperer W.G.; Marquart, T.A. High-nuclearity oxomolybdenum(V) complexes. *Coord. Chem. Rev*. **1993**, *128*, 209–224.

(9) (a) Amor, F.; Gómez-Sal, P.; de Jesús, E.; Martín, A.; Pérez, A. I.; Royo, P.; Vázquez de Miguel, A. Dimetallic Imido Complexes of Molybdenum and Tungsten with Bridged Bis(η5-cyclopentadienyl) Ligands. Molecular Structure of $[(MoO)_2(\mu\text{-}N^tBu)_2\{\mu\text{-}(\eta^5\text{-}C_5H_4)_2SiMe_2\}]$. *Organometallics* **1996**, *15*, 2103–2107. (b) Mathur, P.; Ghose, S.; Hossain, M. M.; Vahrenkamp, H. Synthesis and Structural Characterization of a New μ_2-Te Bridged Complex of Molybdenum with Oxo and Imido Ligands. *J. Organomet. Chem.* **1997**, *538*, 185–188. (c) Edelblut, A. W.; Wentworth, R. A. D. Formation of $Mo_2O_3(NH)(S_2P(OEt)_2)_2$, A Complex with a Bridging Imido Ligand, and its Reactions with Acids. *Inorg. Chem*., **1980**, *19*, 2006–2010. (d) Fletcher, J.; Hogarth, G.; Tocher, D. A. Dimolybdenum Oxo-Imido Complexes: Reactivity of $[(MeC_5H_4)_2Mo_2O_2(\mu\text{-}O)(\mu\text{-}NPh)]$ and Crystal Structure of $[(MeC_5H_4)_2Mo_2O(S)(\mu\text{-}O)(\mu\text{-}NPh)]$. *J. Organomet. Chem.* **1991**, *405*, 207–215. (e) Margulieux, G. W.; Turner, Z. R.; Chirik, P. J. Synthesis and Ligand Modification Chemistry of a Molybdenum Dinitrogen Complex: Redox and Chemical Activity of a Bis-(imino)pyridine Ligand. *Angew. Chem. Int. Ed*. **2014**, *53*, 14211–14215.

(10) (a) Murdzek J. S.; Schrock, R. R. Well-Characterized Olefin Metathesis Catalysts that Contain Molybdenum. *Organometallics* **1987**, *6*, 1373–1374. (b) Nugent, W. A. Synthesis of some d^0 Organoimido Complexes of the Early Transition Metals. *Inorg. Chem*. **1983**, *22*, 965–969. (c) Ma,Y.; Demou , P.; Faller, J. W. A Tungsten-183 NMR study of Mononuclear tungsten(VI) Methyl

Complexes Containing Terminal oxo, sulfido, and imido ligands. *Inorg. Chem*. **1991**, *30*, 62–64. (d) Dahl, L. F.; Frisch, P. D.; Gust, G. R. Synthesis, Structure, and Bonding of a Sulfur-Bridged Alkyl Imido Dimeric Complex of Molybdenum(V). *J. Less-Common Met.* **1974**, *36*, 255–264. (e) Hansen, N. A. K.; Herrmann, W. A. Controlled Thermolysis of Nitrido- and Imidomolybdenum Complexes: A New Route to Phase-Pure Molybdenum Nitrides. *Chem. Mater*. **1998**, *10*, 1677–1679. (f) Coffey, T. A.; Forster, G. D.; Hogarth, G. Synthesis and Molecular Structure of the Molybdate-Bridged Cyclic Imido Complex $[Mo(S_2CNEt_2)_2(NR)(\mu\text{-}MoO_4)]_2$ (R = 2, 6- $^{i}Pr_2C_6H_3$). *Inorg. Chim. Acta* **1998**, *274*, 243–246. (g) Topaloglu-Sozuer, I.; Dulger Irdem, S; Jeffery, J. J.; Hamidov, H. Synthesis, Spectroscopic Characterization and X-ray Crystal structures of Oxo-Bridged Oxo(haloaryl) Imido Hydrotris(3, 5-dimethylpyrazolyl) borate Molybdenum(V) Complexes. *J. Coord. Chem.*, **2005**, *58*, 175–187. (h) Arae, S.; Nakajima, K.; Takahashi, T.; Ogasawara, M. Enantioselective Desymmetrization of 1,2,3-Trisubstituted Metallocenes by Molybdenum-Catalyzed Asymmetric Intraannular Ring-Closing Metathesis. *Organometallics* **2015,** *34*, 1197–1202. (i) Hock, A. S.; Schrock, R. R.; Hoveyda, A. H. Dipyrrolyl Precursors to Bisalkoxide Molybdenum Olefin Metathesis Catalysts. *J. Amer. Chem. Soc.* **2006,** *128*, 16373–16375.

(11) Rosenberg, B.; Vancamp, L.; Trosko, J. E.; Mansour, V. H. Platinum Compounds: a New Class of Potent Antitumour Agents. *Nature* **1969**, *222*, 385–386.

(12) Manegold, C.; Gatzemeier, U.; von Pawel, J.; Pirker, R.; Malayeri, R.; Blatter, J.; Krejcy, K. Front-line Treatment of Advanced Non-small-cell Lung Cancer with MTA (LY231514, Pemetrexed Disodium, ALIMTA™ and Cisplatin: A multicenter phase II Trial. *Ann. Oncol*. **2000,** *11*, 435–440.

(13) Jamieson, E. R.; Lippard, S. J. Structure, Recognition, and Processing of Cisplatin(a) -DNA Adducts. *Chem. Rev.* **1999,** *99*, 2467–2498. (b) Wu, Z.; Liu, Q.; Liang, X.; Yang, X.; Wang, N.; Wang, X.; Sun, H.; Lu, Y.; Guo, Z. Reactivity of Platinum-Based Antitumor Drugs Towards a Met-

and His-rich 20mer Peptide Corresponding to the N-terminal Domain of Human Copper Transporter 1. *J. Biol. Inorg. Chem.* **2009,** *14*, 1313–1323. (c) Jung, Y.; Lippard, S. J. Direct Cellular Responses to Platinum-Induced DNA Damage. *Chem. Rev.* **2007,** *107*, 1387–1407.

(14) Esteban-Fernandez, D.; Moreno-Gordaliza, E.; Canas, B.; Antonia Palacios, M.; Milagros Gomez-Gomez, M. Analytical methodologies for metallomics studies of antitumor Pt-containing drugs. *Metallomics*, **2010**, *2*, 19–38.

(15) Fuertes, M. A.; Alonso, C.; Pérez, J. M. Biochemical Modulation of Cisplatin Mechanisms of Action: Enhancement of Antitumor Activity and Circumvention of Drug Resistance. *Chem. Rev.* **2003**, *103*, 645–662.

(16) Ronconi, L.; Sadler, P. J. Using coordination chemistry to design new medicines. *Coord. Chem. Rev*. **2007**, *251*, 1633–1648.

(17) Rajendiran, V.; Karthik, R.; Palaniandavar, M.; Periasamy, V. S.; Akbarsha, M. A.; Srinag, B. S.; Krishnamurthy, H. Mixed-Ligand Copper(II)-phenolate Complexes: Effect of Coligand on Enhanced DNA and Protein Binding, DNA Cleavage, and Anticancer Activity. *Inorg. Chem.* **2007,** *46*, 8208–8221.

(18) Giannicchi, I.; Brissos, R.; Ramos, D.; Lapuente, J. d.; Lima, J. C.; Cort, A. D.; Rodríguez, L. Substituent Effects on the Biological Properties of Zn-Salophen Complexes. *Inorg. Chem.* **2013**, *52*, 9245–9253.

(19) Bhattacharya, S.; Mandal, S. S. DNA Cleavage by Intercalatable Cobalt–Bispicolylamine Complexes Activated by Visible Light. *Chem. Commun*. **1996**, 1515–1516.

(20) Czlapinski, J. L.; Sheppard, T. L. Nucleic Acid Template-Directed Assembly of Metallosalen−DNA Conjugates. *J. Am. Chem. Soc.* **2001**, *123*, 8618–8619.

(21) Muller, J. G.; Paikoff, S. J.; Rokita, S. E.; Burrows, C. J. DNA Modification Promoted by Water-Soluble Nickel(II) Salen complexes: A switch to DNA alkylation. *J. Inorg. Biochem.* **1994**, *54*, 199–206.

(22) (a) Ansari, K. I.; Grant, J. D.; Kasiri, S.; Woldemaram, G. A.; Shrestha, B.; Mandal, S. S. Manganese(III)-salens induce tumor selective apoptosis in human cells. *J. Inorg. Biochem.* **2009**, *103*, 818–826. (b) Arola-Arnal, A.; Benet-Buchholz, J.; Neidle, S.; Vilar, R. Effects of Metal Coordination Geometry on Stabilization of Human Telomeric Quadruplex DNA by Square-Planar and Square-Pyramidal Metal Complexes. *Inorg. Chem.* **2008,** *47*, 11910–11919. (c) Clever, G. H.; Söltl, Y.; Burks, H.; Spahl, W.; Carell, T., Metal–Salen-Base-Pair Complexes Inside DNA: Complexation Overrides Sequence Information. *Chem. Eur. J.* **2006,** *12*, 8708–8718. (d) Ansari, K. I.; Grant, J. D.; Woldemaram, G. A.; Kasiri, S.; Mandal, S. S. Iron(III)-salen Complexes with Less DNA cleavage Activity Exhibit More Efficient Apoptosis in MCF7 cells. *Org. Biomol. Chem.* **2009**, *7*, 926–932.

(23) Ansari, K. I.; Kasiri, S.; Grant, J. D.; Mandal, S. S. Apoptosis and Anti-Tumour Activities of Manganese(III)-Salen and -Salphen Complexes. *Dalton Trans.* **2009**, 8525–8531.

(24) Vrdoljak, V.; Đilović, I.; Rubčić, M.; Kraljević Pavelić, S.; Kralj, M.; Matković–Čalogović, D.; Piantanida, I.; Novak, P.; Rožman, A.; Cindrić, M. Synthesis and Characterisation of Thiosemicarbazonato Molybdenum(VI) Complexes and their In Vitro Antitumor Activity. *Eur. J. Med. Chem.* **2010**, *45*, 38–48.

(25) Bandarra, D.; Lopes, M.; Lopes, T.; Almeida, J.; Saraiva, M. S.; Vasconcellos-Dias, M.; Nunes, C. D.; Félix, V.; Brandão, P.; Vaz, P. D.; Meireles, M.; Calhorda. Mo(II) complexes: A New Family of Cytotoxic Agents? *J. Inorg. Biochem.*, **2010**, *104*, 1171–1177.

(26) Mrózek, O.; Šebestová, L.; Vinklárek, J.; Řezáčová, M.; Eisner, A.; Růžičková, Z.; Honzíček, J. Highly Water-Soluble Cyclopentadienyl and Indenyl Molybdenum(II) Complexes – Second Generation of Molybdenum-Based Cytotoxic Agents. *Eur. J. Inorg. Chem.* **2016**, 519–529.

(27) Harding, M. M.; Mokdsi, G.; Mackay, J. P.; Prodigalidad, M.; Lucas, S. W. Interactions of the Antitumor Agent Molybdocene Dichloride with Oligonucleotides. *Inorg. Chem.* **1998**, *37*, 2432–2437.

(28) Narváez-Pita, X.; Ortega-Zuniga, C.; Acevedo-Morantes, C. Y.; Pastrana, B.; Olivero-Verbel, J.; Maldonado-Rojas, W.; Ramírez-Vick, J. E.; Meléndez, E. Water Soluble Molybdenocene Complexes: Synthesis, Cytotoxic Activity and Binding Studies to Ubiquitin by Fluorescence Spectroscopy, Circular Dichroism and Molecular Modeling. *J. Inorg. Biochem.* **2014**, *132*, 77–91.

(29) Gleeson, B.; Claffey, J.; Deally, A.; Hogan, M.; Méndez, L. M. M.; Müller-Bunz, H.; Patil, S.; Tacke, M. Novel Benzyl-Substituted Molybdocene Anticancer Drugs. *Inorg. Chim. Acta* **2010**, *363*, 1831–1836.

(30) Harding, M. M.; Harden, G. J.; Field, L. D. A ^{31}P NMR Study of the Interaction of the Antitumor Active Metallocene Cp_2MoCl_2 with calf thymus DNA. *FEBS Lett.* **1993**, *322*, 291–294.

(31) Feng, J.; Lu, X.-m.; Wang, G.; Du, S.-z.; Cheng, Y.-f. The Syntheses and Characterizations of Molybdenum(VI) complexes with Catechol and 2,3-Dihydroxynaphthalene, and the Structure–Effect Relationship in their *in vitro* Anticancer Activities. *Dalton Trans.* **2012,** *41*, 8697–8702.

(32) Cindrić, M.; Novak, T. K.; Kraljević, S.; Kralj, M.; Kamenar, B. Structural and Antitumor Activity Study of γ-Octamolybdates Containing Aminoacids and Peptides. *Inorg. Chim. Acta* **2006**, *359*, 1673–1680.

(33) Zhang, K.; Cui, S.; Wang, J.; Wang, X.; Li, R. Study on Antitumor Activity of Metal-Based Diketone Complexes. *Med. Chem. Res.* **2012**, *21*, 1071–1076.

(34) Saraiva, M. S.; Quintal, S.; Portugal, F. C. M.; Lopes, T. A.; Félix, V.; Nogueira, J. M. F.; Meireles, M.; Drew, M. G. B.; Calhorda, M. J. Nitrogen Donor Ligands Bearing N–H Groups: Effect on Catalytic and Cytotoxic Activity of Molybdenum η^3-Allyldicarbonyl Complexes. *J. Organomet. Chem.* **2008**, *693*, 3411–3418.

(35) (a) Rao, N. S.; Mishra, D. D.; Maurya, R. C.; Rao, N. N. Synthesis and Characterisation of Some Novel CIS-Dioxo-Molybdenum (VI) Complexes of Schiff Bases Derived from Salicylaldehyde. *Synth. React. Inorg. Met.-Org. Chem*. **1995**, *25*, 437–449. (b) Hill, W. E.; Atabay, N.; McAuliffe, C. A.; McCullough, F. P.; Razzoki, S. M. The coordination chemistry of Molybdenum and Tungsten. Part XIV. Dioxomolybdenum(VI) Complexes of Bidentate, Tridentate, and Tetradentate Schiff Bases Containing Oxygen, Nitrogen and Sulphur Donors. *Inorg. Chim. Acta* **1979**, *35*, 35–41. (c) El-Medani, S. M.; Ali, O. A. M.; Ramadan, R. M. Photochemical Reactions of Group 6 Metal Carbonyls with N-Salicylidene-2-Hydroxyaniline and Bis-(salicylaldehyde)phenylenediimine. *J. Mol. Struct.* **2005**, *738*, 171–177. (d) Tarafder, M. T. H.; Khan, A. R. Peroxo Complexes of Zirconium(IV), Thorium(IV), Molybdenum(VI), Tungsten(VI) and Uranium(VI) Containing Two Quadridentate ONNO Schiff Bases. *Polyhedron* **1991**, *10*, 819–822.

(36) (a) Bruno, S. M.; Balula, S. S.; Valente, A. A.; Almeida Paz, F. A.; Pillinger, M.; Sousa, C.; Klinowski, J.; Freire, C.; Ribeiro-Claro, P.; Gonçalves, I. S. Synthesis and Catalytic Properties in Olefin Epoxidation of Dioxomolybdenum(VI) Complexes Bearing a Bidentate or Tetradentate Salen-Type Ligand. *J. Mol. Catal. A: Chem*. **2007**, *270*, 185–194. (b) Schilf, W.; Kamieński, B.; Rozwadowski, Z.; Ambroziak, K.; Bieg, B.; Dziembowska, T. Solid State ^{15}N and ^{13}C NMR Study of Dioxomolybdenum (VI) Complexes of Schiff Bases Derived From Trans-1,2-Cyclohexanediamine. *J. Mol. Struct.* **2004,** *700*, 61–65. (c) Cameron, J. H.; McEwan, J. A.

Tridentate Coordination of Dioxomolybdenum(VI) with Some Potentially Quinquedentate (N_2O_3) Schiff Base Ligands. *Inorg. Chim. Acta* **1993,** *211*, 111–116.

(37) (a) Schley, M.; Fritzsche, S.; Lonnecke, P.; Hey-Hawkins, E. Soluble Monometallic Salen Complexes Derived from O-Functionalised Diamines as Metalloligands for the Synthesis of Heterobimetallic Complexes. *Dalton Trans.* **2010**, *39*, 4090–4106. (b) Judmaier, M. E.; Holzer, C.; Volpe, M.; Mösch-Zanetti, N. C. Molybdenum(VI) Dioxo Complexes Employing Schiff Base Ligands with an Intramolecular Donor for Highly Selective Olefin Epoxidation. *Inorg. Chem.* **2012,** *51*, 9956–9966. (c) Pandhare, S. L.; Jadhao, R. R.; Puranik, V. G.; Joshi, P. V.; Capet, F.; Dongare, M. K.; Umbarkar, S. B.; Michon, C.; Agbossou-Niedercorn, F. Molybdenum(VI) Dioxo Complexes for the Epoxidation of Allylic Alcohols and Olefins. *J. Organomet. Chem.* **2014,** *772–773*, 271–279.

(38) (a) Dash, S. P.; Pasayat, S.; Bhakat, S.; Roy, S.; Dinda, R.; Tiekink, E. R. T.; Mukhopadhyay, S.; Bhutia, S. K.; Hardikar, M. R.; Joshi, B. N.; Patil, Y. P.; Nethaji, M. Highly Stable Hexacoordinated Nonoxidovanadium(IV) Complexes of Sterically Constrained Ligands: Syntheses, Structure, and Study of Antiproliferative and Insulin Mimetic Activity. *Inorg. Chem.* **2013**, *52*, 14096–14107. (b) Pasayat, S.; Dash, S. P.; Majumder, S.; Dinda, R.; Sinn, E.; Stoeckli-Evans, H.; Mukhopadhyay, S.; Bhutia, S. K.; Mitra, P. Synthesis, Structure, Characterization and Study of Antiproliferative Activity of Dimeric and Tetrameric Oxidomolybdenum(VI) Complexes of N,N′-disalicyloylhydrazine. *Polyhedron*, **2014**, *80*, 198–205. (c) Saswati; Chakraborty, A.; Dash, S. P.; Panda, A. K.; Acharyya, R.; Biswas, A.; Mukhopadhyay, S.; Bhutia, S. K.; Crochet, A.; Patil, Y. P.; Nethaji, M.; Dinda, R Synthesis, X-ray Structure and *in vitro* Cytotoxicity Studies of Cu(I/II) Complexes of Thiosemicarbazone: Special Emphasis on their Interactions with DNA. *Dalton Trans.* **2015**, *44*, 6140–6157. (d) Dash, S. P.; Panda, A. K.; Pasayat, S.; Majumder, S.; Biswas, A.; Kaminsky, W.; Mukhopadhyay, S.; Bhutia, S. K.; Dinda, R. Evaluation of the Cell Cytotoxicity and DNA/BSA Binding and Cleavage Activity of some Dioxidovanadium(V) Complexes Containing

Aroylhydrazones. *J. Inorg. Biochem.* **2015**, *144*, 1–12. (e) Dash, S. P.; Panda, A. K.; Pasayat, S.; Dinda, R.; Biswas, A.; Tiekink, E. R. T.; Mukhopadhyay, S.; Bhutia, S. K.; Kaminsky, W.; Sinn, E. Oxidovanadium(V) Complexes of Aroylhydrazones Incorporating Heterocycles: Synthesis, Characterization and Study of DNA Binding, Photoinduced DNA Cleavage and Cytotoxic Activities. *RSC Adv.* **2015**, *5*, 51852–51867. (f) Dash, S. P.; Panda, A. K.; Pasayat, S.; Dinda, R.; Biswas, A.; Tiekink, E. R. T.; Patil, Y. P.; Nethaji, M.; Kaminsky, W.; Mukhopadhyay, S.; Bhutia, S. K. Syntheses and Structural Investigation of Some Alkali Metal Ion-Mediated $L^{V}VO^{2-}$ (L^{2-} = tridentate ONO ligands) Species: DNA Binding, Photoinduced DNA Cleavage and Cytotoxic Activities. *Dalton Trans.* **2014**, *43*, 10139–10156. (g) Dash, S. P.; Panda, A. K.; Dhaka, S.; Pasayat, S.; Biswas, A.; Maurya, M. R.; Majhi, P. K.; Crochet, A.; Dinda, R. A Study of DNA/BSA Interaction and Catalytic Potential of Oxidovanadium(V) Complexes with ONO Donor ligands. *Dalton Trans.* **2016,** *45*, 18292–18307.

(39) Mandal, S.; Mandal, S.; Seth, D. K.; Mukhopadhyay, B.; Gupta, P. Ruthenium and Osmium Complexes of Novel Carbohydrate Derived Salen Ligands: Synthesis, Characterization and *in situ* Ligand Reduction. *Inorg. Chim. Acta* **2013**, *398*, 83–88.

(40) (a) Minato, M.; Fujiwara, Y.; Koga, M.; Matsumoto, N.; Kurishima, S.; Natori, M.; Sekizuka, N.; Yoshioka, K.-i.; Ito, T. Reductions of C=O and C=N groups With the Systems Composed of $(\eta^5\text{-}C_5H_5)_2MoH_2$ and Acids. *J. Organomet. Chem.* **1998**, *569*, 139–145.

(41) (a) Maurya, M. R.; Kumar, A.; Ebel, M.; Rehder, D. Synthesis, Characterization, Reactivity, and Catalytic Potential of Model Vanadium(IV, V) Complexes with Benzimidazole-Derived ONN Donor Ligands. *Inorg. Chem*. **2006**, *45*, 5924–5937. (b) Bertini, S.; Coletti, A.; Floris, B.; Conte, V.; Galloni, P. Investigation of VO–Salophen Complexes Electronic structure. *J. Inorg. Biochem*. **2015**, *147*, 44–53. (c) Tzubery, A.; Tshuva, E. Y. Trans Titanium(IV) Complexes of Salen Ligands Exhibit High Antitumor Activity. *Inorg. Chem.* **2011**, *50*, 7946–7948. (d) Castro-Osma, J. A.;

Lamb, K. J.; North, M. Cr(salophen) Complex Catalyzed Cyclic Carbonate Synthesis at Ambient Temperature And Pressure. *ACS Catal.* **2016**, *6*, 5012–5025. (e) Bhowmik, P.; Nayek, H. P.; Corbella, M.; Aliaga-Alcalde, N.; Chattopadhyay, S. Control of Molecular Architecture by Steric Factors: Mononuclear vs Polynuclear Manganese(III) Compounds with Tetradentate N_2O_2 Donor Schiff Bases. *Dalton Trans.* **2011**, *40*, 7916–7926. (f) Jana, S.; Chatterjee, S.; Chattopadhyay, S. Syntheses, Characterization and X-ray Crystal Structures of Hexa-Coordinated Monomeric and Oxo-Bridged Dimeric Fe(III) Compounds with Salen-type Schiff Bases. *Polyhedron* **2012**, *48*, 189–198. (g) Amirnasr, M.; Schenk, K. J.; Gorji, A.; Vafazadeh, R. Synthesis and Spectroscopic Characterization of $[Co^{III}(salophen)(amine)_2]ClO_4$ (amine=morpholine, pyrrolidine, and piperidine) complexes. The crystal structures of $[Co^{III}(salophen)(morpholine)_2]ClO_4$ and $[Co^{III}(salophen)(pyrrolidine)_2]ClO_4$. *Polyhedron* **2001**, *20*, 695–702. (h) de Bellefeuille, D.; Askari, M. S.; Lassalle-Kaiser, B.; Journaux, Y.; Aukauloo, A.; Orio, M.; Thomas, F.; Ottenwaelder, X. Reversible Double Oxidation and Protonation of the Non-Innocent Bridge in a Nickel(II) Salophen Complex. *Inorg. Chem.* **2012**, *51*, 12796–12804. (i) de Bellefeuille, D.; Orio, M.; Barra, A.-L.; Aukauloo, A.; Journaux, Y.; Philouze, C.; Ottenwaelder, X.; Thomas, F. Redox Noninnocence of the Bridge in Copper(II) Salophen and Bis(oxamato) Complexes. *Inorg. Chem.* **2015**, *54*, 9013–9026. (j) Escudero-Adán, E. C.; Benet-Buchholz, J.; Kleij, A. W. Expedient Method for the Transmetalation of Zn(II)-Centered Salphen Complexes. *Inorg. Chem.* **2007**, *46*, 7265–7267. (k) Wong, T.-W.; Lau, T.-C.; Wong, W.-T. Osmium(VI) Nitrido and Osmium(IV) Phosphoraniminato Complexes Containing Schiff Base Ligands. *Inorg. Chem.* **1999**, *38*, 6181–6186. (l) Proetto, M. T.; Liu, W.; Molchanov, A.; Sheldrick, W. S.; Hagenbach, A.; Abram, U.; Gust, R. Synthesis, Characterization, and in vitro Antiproliferative Activity of [Salophene]platinum(II) Complexes. *ChemMedChem* **2014**, *9*, 1176–1187.

(42) Chen, G. J. J.; McDonald, J. W.; Newton, W. E. Synthesis of Molybdenum(IV) and Molybdenum(V) Complexes using Oxo Abstraction by Phosphines. Mechanistic Implications. *Inorg. Chem.* **1976**, *15*, 2612–2615.

(43) Choudhary, N. F.; G. Connelly, N.; B. Hitchcock, P.; Jeffery Leigh, G. New Compounds of Tetradentate Schiff Bases with Vanadium(IV) and Vanadium(V). *J. Chem. Soc., Dalton Trans.* **1999**, 4437–4446.

(44) Ding, L.; Jin, W.; Chu, Z.; Chen, L.; Lü, X.; Yuan, G.; Song, J.; Fan, D.; Bao, F. Bulk Solvent-Free Melt Ring-Opening Polymerization (ROP) of L-Lactide Catalyzed by Ni(II) and Ni(II)–Ln(III) Complexes Based on the Acyclic Salen-Type Schiff-Base Ligand. *Inorg. Chem. Commun.* **2011**, *14*, 1274–1278.

(45) (a) Bruker **2007** *APEX2* (Version 2.1-4); *SAINT* (version 7.34A); *SADABS* (version2007/4); BrukerAXS Inc, Madison, Wisconsin, USA. (b) Sheldrick, G. M.; *SHELXS-97*, Program for Crystal Structure Determination, Universität Göttingen, Göttingen, Germany, 1997.

(46) (a) Sheldrick, G. M. *SHELXL-97*, Program for Refinement of Crystal Structures, Universität Göttingen, Göttingen, Germany, 1997. (b) Mackay, S.; Edwards, C.; Henderson, A.; Gilmore, C.; Stewart, N.; Shankland, K.; Donald, A. **1997** MaXus: A computer program for the solution and refinement of crystal structures from diffraction data. University of Glasgow, Scotland.

(47) (a) Kumar, P.; Gorai, S.; Kumar Santra, M.; Mondal, B.; Manna, D. DNA Binding, Nuclease Activity and Cytotoxicity Studies of Cu(II) Complexes of Tridentate Ligands. *Dalton Trans*. **2012**, *41*, 7573–7581. (b) Suzuki, T.; Fujikura, K.; Higashiyama, T.; Takata, K. DNA Staining for Fluorescence and Laser Confocal Microscopy. *J. Histochem. Cytochem.* **1997**, *45*, 49–53. (c) Pasayat, S.; Böhme, M.; Dhaka, S.; Dash, S. P.; Majumder, S.; Maurya, M. R.; Plass, W.; Kaminsky, W.; Dinda, R. Synthesis, Theoretical Study and Catalytic Application of Oxidometal (Mo or V) Complexes: Unexpected Coordination Due to Ligand Rearrangement through Metal-

Mediated C–C Bond Formation. *Eur. J. Inorg. Chem.* **2016**, 1604–1618. (d) Brondino, C. D.; Rivas, M. G.; Romão, M. J.; Moura, J. J. G.; Moura, I. Structural and Electron Paramagnetic Resonance (EPR) Studies of Mononuclear Molybdenum Enzymes from Sulfate-Reducing Bacteria. *Acc. Chem. Res.* **2006**, *39*, 788−796. (e) Yang, Z.; Gould, E. S. Reactions of molybdenum(VI) with metal ion reductants. *Dalton Trans.* **2006**, 3427–3430. (f) Martell A. E. Vitamin B_6 Catalyzed Reactions of a-Amino and a-Keto Acids: Model Systems. *Acc. Chem. Res*. **1989**, *22*, 115−124 (g) Cavaco, I.; Pessoa, J. C.;. Luz, S.M; Duarte, M. T. N-Salicylideneamino-acidate complexes of oxovanadium(IV)-II. Synthesis, Characterization and Deamination ofan N-Salicylideneglycylclycinato Complex. *Polyhedron* **1995**, *14*, 429–439. (h) Correia, I.; Avecilla, F.; Marcão, S.; Pessoa, J. C. Structural Studies of Decavanadate Compounds with Organic Molecules and Inorganic Ions in Their Crystal Packing. *Inorg. Chim. Acta* **2004**, *357*, 4476–4487. (i) Klein, R. F.X.; Bargas, L. M.; Horak V. Spontaneous Rearrangrment In Corey's Reaction. *Tetrahedron Lett.* **1988**, *29*, 851–852. (j) Young, C. G. Oxomolybdenum Chemistry: An Experiment. *J. Chem. Educ.* **1995**, *72*, 751–753. (k) Young, C. G., Biomimetic Chemistry of Molybdenum. *In Biomimetic Oxidations Catalyzed by Transition Metal Complexes*, Published By Imperial College Press And Distributed By World Scientific Publishing Co. **2011**; pp 415–459.

(48) (a) Nagy, E. M.; Pettenuzzo, A.; Boscutti, G.; Marchiò, L.; Dalla Via, L.; Fregona, D. Ruthenium(II/III)-Based Compounds with Encouraging Antiproliferative Activity against Non-small-Cell Lung Cancer. *Chem. Eur. J.* **2012**, *18*, 14464–14472. (b) Melby, L. R. Crystalline Molybdenum(V)-Histidine Complex. *Inorg. Chem.* **1969**, *8*, 1539–1540. (c) Spence, J. T.; Lee, J. Y. Histidine Complexes of Molybdenum(V) and Molybdenum(VI). *Inorg. Chem.* **1965**, *4*, 385–388.

(49) (a) Dinda, R.; Sengupta, P.; Ghosh, S.; Sheldrick, William S. Synthesis, Structure, and Reactivity of a New Mononuclear Molybdenum(VI) Complex Resembling the Active Center of Molybdenum Oxotransferases. *Eur. J. Inorg. Chem.* **2003**, 363–369. (b) Dinda, R.; Ghosh, S.;

Falvello, L. R.; Tomás, M.; Mak, T. C. W. Synthesis, Structure, and Reactivity of Some New Dipyridyl and Diamine-Bridged Dinuclear Oxomolybdenum(VI) Complexes. *Polyhedron* **2006**, *25*, 2375–2382. (c) Dinda, R.; Sengupta, P.; Ghosh, S.; Mayer-Figge, H.; Sheldrick, W. S. A family of Mononuclear Molybdenum-(VI), and -(IV) Oxo Complexes with a Tridentate (ONO) Ligand. *J. Chem. Soc., Dalton Trans.* **2002**, 4434–4439. (d) Basu P.; Nemykin V. N.; Sengar R. S; Syntheses, Spectroscopy, and Redox Chemistry of Encapsulated Oxo−Mo(V) Centers: Implications for Pyranopterin-Containing Molybdoenzymes. *Inorg.Chem.*, **2003**, *42*, 7489–7501 (e) Huang T. J.; Haight G. P. Jr. Paramagnetic Monomeric Molybdenum (V) –Cysteine Complex as a Model for Molybdenum-Enzyme Interaction. *J. Am. Chem. Soc.*, **1970**, *92*, 2336–2342. (f) Bellefeuille, D. de.; Askari, M. S.; Lassalle-Kaiser, B.; Journaux, Y.; Aukauloo, A.; Orio, M.; Thomas, F.; Ottenwaelder X. *Inorg. Chem*. **2012**, *51*, 12796−12804.

(50) (a) Bermejo, M. R.; Fernández, M. I.; González-Noya, A. M.; Maneiro, M.; Pedrido, R.; Rodríguez, M. J.; García-Monteagudo, J. C.; Donnadieu, B. Novel Peroxidase Mimics: μ-Aqua Manganese–Schiff Base Dimers. *J. Inorg. Biochem*. **2006**, *100*, 1470–1478. (b) Bermejo, M. R.; Fernández, M. I.; Gómez-Fórneas, E.; González-Noya, A.; Maneiro, M.; Pedrido, R.; Rodríguez, M. J. Self-Assembly of Dimeric Mn^{III}–Schiff-Base Complexes Tuned by Perchlorate Anions. *Eur. J. Inorg. Chem.* **2007**, 3789–3797.

(51) (a) Bray, R. C. EPR of Molybdenum-Containing Enzymes. In *Biological Magnetic Resonance*; Berliner, L. J., Reuben, J., Ed.; Plenum Press: New York, 1980; *Vol. 2*, pp 45–84. (b) Hanson, G. R.; Noble, C. J.; Benson, S. Molecular Sophe: An Integrated Approach to the Structural Characterization of Metalloproteins: The Next Generation of Computer Simulation Software. In *High Resolution EPR: Applications to Metalloenzymes and Metals in Medicine*; Berliner, L., Hanson, G., Ed.; Springer New York: New York, 2009; pp 105–173. (c) Chang, C. S. J.; Collison, D.; Mabbs, F. E.; Enemark, J. H. Synthesis and Characterization of Mononuclear

Oxomolybdenum(V) Complexes with Aliphatic Diolato, Dithiolato, or Alkoxo Ligands: Effect of Chelate Ring Size on the Properties of the Metal Center. *Inorg. Chem.* **1990**, *29*, 2261–2267.

(52) (a) Bose, M.; Moula, G.; Sarkar, S. Mono(maleonitriledithiolene) molybdenum(IV) and Bis(μ-sulfido)-Bridged Dimolybdenum(V) Complexes with Mo=S Moiety. *Chem. Biodiversity* **2012**, *9*, 1867–1879 (b) Modec, B.; Šala, M.; Clérac, R. Clérac Pyrazine-Assisted Dimerization of Molybdenum(V): Synthesis and Structural Characterization of Novel Dinuclear and Tetranuclear Complexes. *Eur. J. Inorg. Chem.* **2010**, 542–553. (c) Mandal, D.; Ganguly, R.; Chatterjee, P. B.; Endo, A.; Weakley, T. J. R.; Chaudhury, M. Cis-Dioxomolybdenum(VI) Complexes of Sterically Encumbered Phenol-based Tetradentate N_2O_2 Ligands: Structural, Spectroscopic, and Electrochemical studies. *Struct. Chem*. **2007**, *18*, 187–193.

(53) (a) Bhattacharya, K.; Abtab, S. M. T.; Majee, M. C.; Endo, A.; Chaudhury, M. Targeted Synthesis of Heterobimetallic Compounds Containing a Discrete Vanadium(V)−μ-Oxygen–Iron(III) Core. *Inorg. Chem*. **2014**, *53*, 8287–8297. (b) Conry R. R.; Tipton A. A. A mononuclear molybdenum(V) mono-oxo biphenyl-2,2'-dithiolate complex in which the metal resides within a cleft formed by the ligands and that exhibits N-H···S hydrogen bonding in the solid state. *J. Biol. Inorg. Chem.* **2001**, *6*, 359–366. (c) Bradbury, J. R.; Masters, A. F.; McDonell, A. C.; Brunette, A. A.; Bond, A. M.; Wedd A. G. Redox Properties of Thiolate Compounds of Oxomolybdenum(V) and Their Tungsten and Selenium Analogues. *J. Am. Chem. Soc.* **1981**,*103*, 1959–1964. (d) Bellefeuille, D. de.; Askari, M. S.; Lassalle-Kaiser, B.; Journaux, Y.; Aukauloo, A.; Orio, M.; Thomas, F.; Ottenwaelder X. Reversible Double Oxidation and Protonation of the Non-Innocent Bridge in a Nickel(II) Salophen Complex. *Inorg. Chem.* **2012**, *51*, 12796−12804.

(54) Parimala, S.; Selvam, P. Crystal structure of aquadioxido-(2-{[(2-oxidoethyl)imino]methyl}phenolato-κ^3 O,N,O′)molybdenum(VI). *Acta Crystallogr. Sect. E.* **2015**, *71*, m35–m36.

(55) (a) Hille, R. The Mononuclear Molybdenum Enzymes. *Chem. Rev*. **1996**, *96*, 2757–2816. (b) Romão, M. J.; Archer, M.; Moura, I.; Moura, J. J. G.; LeGall, J.; Engh, R.; Schneider, M.; Hof, P.; Huber, R. Huber, Crystal Structure of the Xanthine Oxidase-Related Aldehyde Oxido-Reductase from D. gigas. *Science* **1995**, *270*, 1170–1176.

(56) Modec, B.; Brenčič, J. V.; Finn, R. C.; Rarig, R. S.; Zubieta, J. Structural Isomerism Among Octanuclear Oxomolybdenum(V) Coordination Compounds with Pyridines. Two Isomers of $[Mo_8O_{16}(OCH_3)_8(R–Py)_4]$. *Inorg. Chim. Acta* **2001**, *322*, 113–119.

(57) (a) Pasayat, S.; Dash, S. P.; Saswati; Majhi, P. K.; Patil, Y. P.; Nethaji, M.; Dash, H. R.; Das, S.; Dinda, R. Mixed-Ligand Aroylhydrazone Complexes of Molybdenum: Synthesis, Structure and Biological Activity. *Polyhedron* **2012**, *38*, 198–204. (b) Pasayat, S.; Dash, S. P.; Roy, S.; Dinda, R.; Dhaka, S.; Maurya, M. R.; Kaminsky, W.; Patil, Y. P.; Nethaji, M. Synthesis, Structural Studies and Catalytic Activity of Dioxidomolybdenum(VI) Complexes with Aroylhydrazones of Naphthol-Derivative. *Polyhedron* **2014**, *67*, 1–10.

(58) (a) Subramanian, P.; Spence, J. T.; Ortega, R.; Enemark, J. H. Molybdenum(VI)-dioxo Complexes with Sterically Bulky Ligands. *Inorg. Chem*. **1984**, *23*, 2564–2572. (b) Dupe, A.; Judmaier, M. E.; Belaj, F.; Zangger, K.; Mosch-Zanetti, N. C. Activation of Molecular Oxygen by a Molybdenum Complex for Catalytic Oxidation. *Dalton Trans*. **2015**, *44*, 20514–20522.

(59) Arjmand, F.; Mohani, B.; Ahmad, S. Synthesis, Antibacterial, Antifungal Activity and Interaction of CT-DNA with a New Benzimidazole Derived Cu(II) Complex. *Eur. J. Med. Chem*. **2005**, *40*, 1103–1110.

(60) Rajendiran, V.; Murali, M.; Suresh, E.; Sinha, S.; Somasundaram, K.; Palaniandavar. Mixed Ligand Ruthenium(II) Complexes of Bis(pyrid-2-yl)-/Bis(Benzimidazol-2-yl)-Dithioether and Diimines: Study of Non-Covalent DNA Binding and Cytotoxicity. *Dalton Trans.* **2008**, 148–163.

(61) Arjmand, F.; Aziz, M. Synthesis and Characterization of Dinuclear Macrocyclic Cobalt(II), Copper(II) and Zinc(II) Complexes Derived from 2,2,2′,2′-S,S[Bis(Bis-N,N-2-Thiobenzimidazolyloxalato-1,2-Ethane)]: DNA Binding and Cleavage Studies. *Eur. J. Med. Chem*. **2009**, *44*, 834–844. (b) (b) Neidle, S. DNA minor-groove recognition by small molecules. *Nat. Prod. Rep*. **2001**, *18*, 291−309. (c) Bindu, P. J.; Mahadevan, K. M.; Naik, T. R. R.; Harish, B. G. Synthesis, DNA binding, docking and photocleavage studies of quinolinyl chalcones. *MedChemComm*. **2014**, *5*, 1708−1717. (d) Jeyalakshmi, K.; Arun, Y.; Bhuvanesh, N. S. P.; Perumal, P. T.; Karvembu A. S. R. DNA/protein binding, DNA cleavage, cytotoxicity, superoxide radical scavenging and molecular docking studies of copper(II) complexes containing N-benzyl-N'-aryl-N''-benzoylguanidine ligands. *Inorg. Chem. Front.* **2015**, *2*, 780–798.

(62) (a) An, Y.; Liu, S.-D.; Deng, S.-Y.; Ji, L.-N.; Mao, Z.-W. Cleavage of Double-Strand DNA by Linear and Triangular Trinuclear Copper Complexes. *J. Inorg. Biochem*. **2006**, *100*, 1586−1593; (b) Banerjee, S.; Hussain, A.; Prasad, P.; Khan, I.; Banik, B.; Kondaiah, P.; Chakravarty, A. R. Photocytotoxic Oxidovanadium(IV) Complexes of Polypyridyl Ligands Showing DNA-Cleavage Activity in Near-IR Light. *Eur. J. Inorg. Chem*. **2012**, 3899−3908.

(63) Poklar, N.; Pilch, D. S.; Lippard, S. J.; Redding, E. A.; Dunham, S. U.; Breslauer, K. J. Influence of Cisplatin Intrastrand Crosslinking on the Conformation, Thermal Stability, and Energetics of a 20-mer DNA Duplex. *Proc Natl Acad Sci U S A*. **1996**, *93*, 7606−7611.

(64) (a) Li, L.; Guo, Q.; Dong, J.; Xu, T.; Li, J. DNA Binding, DNA Cleavage and BSA Interaction of a Mixed-Ligand Copper(II) Complex with Taurine Schiff Base and 1,10-Phenanthroline. *Photochem. Photobiol. B*. **2013**, *125*, 56–62.

(65) (a) Dai, W.-M.; Lai, K. W.; Wu, A.; Hamaguchi, W.; Lee, M. Y. H.; Zhou, L.; Ishii, A.; Nishimoto, S.-i. DNA Cleavage Potency, Cytotoxicity, and Mechanism of Action of a Novel Class of Enediyne Prodrugs. *J. Med. Chem*. **2002**, *45*, 758–761.

(66) (a) Kim, J. S.; Gatto, B.; Yu, C.; Liu, A.; Liu, L. F.; LaVoie, E. J. Substituted 2,5'-Bi-1H-benzimidazoles: Topoisomerase I Inhibition and Cytotoxicity. *J. Med. Chem*. **1996**, *39*, 992–998. (b) Sasmal, P. K.; Saha, S.; Majumdar, R.; De, S.; Dighe, R. R.; Chakravarty, A. R. Oxovanadium(IV) Complexes of Phenanthroline Bases: the Dipyridophenazine Complex as a Near-IR Photocytotoxic Agent. *Dalton Trans*. **2010**, *39*, 2147–2158.

(67) (a) Efthimiadou, E. K.; Karaliota, A.; Psomas, G. Mononuclear Dioxomolybdenum(VI) Complexes with the Quinolones Enrofloxacin and Sparfloxacin: Synthesis, Structure, Antibacterial Activity and Interaction with DNA. *Polyhedron* **2008**, *27*, 349–356. (b) Hussein, M. A.; Guan, T. S.; Haque, R. A.; Ahamed, M. B. K.; Majid, A. M. S. A. Synthesis and Characterization of Thiosemicarbazonato Molybdenum(VI) Complexes: In vitro DNA Binding, Cleavage, and Antitumor Activities. *Polyhedron* **2015**, *85*, 93–103. (c) Selim, M.; Saha, A.; Mukherjea, K. K. Synthesis, characterization, and DNA binding of the biologically relevant novel cationic molybdenum(VI)–glutathione complex $[Mo(GS)(Cl)(H_2O)]Cl_2$. *Monatsh. Chem*. **2012**, *143*, 227–233. (d) Ahmadi, S. M.; Dehghan, G.; Hosseinpourfeizi, M. A.; Dolatabadi, J. E. N.; Kashanian, S. Preparation, Characterization, and DNA Binding Studies of Water-Soluble Quercetin–Molybdenum(VI) Complex. *DNA Cell Biol*. **2011**, *30*, 517–523. (e) Anbu, S.; Kandaswamy, M. Electrochemical, Magnetic, Catalytic, DNA Binding and Cleavage Studies of New Mono and Binuclear Copper(II) Complexes. *Polyhedron* **2011**, *30*, 123–131. (f) Selvarani, V.; Annaraj, B.; Neelakantan, M. A.; Sundaramoorthy, S.; Velmurugan, D. Synthesis, Characterization and Crystal Structures of Copper(II) and Nickel(II) Complexes of Propargyl Arm Containing N_2O_2 Ligands: Antimicrobial Activity and DNA Binding. *Polyhedron* **2013**, *54*, 74–83. (g) Arun, T.; Packianathan, S.; Malarvizhi, M.; Antony, R.; Raman, N. Bio-Relevant Complexes of Novel N_2O_2 Type Heterocyclic ligand: Synthesis, Structural Elucidation, Biological Evaluation and Docking Studies. *J. Photochem. Photobiol., B*. **2015**, *149*, 93–102. (h) Mandegani, Z.; Asadi, Z.; Asadi, M.;

Karbalaei-Heidari, H. R.; Rastegari, B. Synthesis, Characterization, DNA Binding, Cleavage Activity, Cytotoxicity and Molecular Docking of New Nano Water-Soluble [M(5-CH_2PPh_3-3,4-salpyr)]$(ClO_4)_2$ (M = Ni, Zn) Complexes. *Dalton Trans*. **2016**, *45*, 6592–6611.

(68) (a) Zhang, L.; Ren, W.; Wang, X.; Zhang, J.; Liu, J.; Zhao, L.; Zhang, X. Discovery of Novel Polycyclic Spiro-Fused Carbocyclicoxindole-Based Anticancer Agents. *Eur. J. Med. Chem.* **2017,** *126*, 1071–1082. (b) Jung, H.; Dubey, A.; Koo, H. J.; Vajpayee, V.; Cook, T. R.; Kim, H.; Kang, S. C.; Stang, P. J.; Chi, Ki-W. Self-Assembly of Ambidentate Pyridyl-Carboxylate Ligands with Octahedral Ruthenium Metal Centers: Self-Selection for a Single-Linkage Isomer and Anticancer-Potency Studies. *Chem. Eur. J.* **2013**, 6709–6717. (c) Ramadan, A. M. Structural and Biological Aspects of Copper (II) Complexes with 2-Methyl-3-Amino-(3–H)-Quinazolin-4-one. *J. Inorg. Biochem*. **1997**, *65*, 183–189.

(69) (a) Avaji, P. G.; Kumar, C. H. V.; Patil, S. A.; Shivananda K. N.; Nagaraju, C. Synthesis, Spectral Characterization, In-Vitro Microbiological Evaluation and Cytotoxic Activities of Novel Macrocyclic Bis Hydrazone. *Eur. J. Med. Chem*. **2009**, *44*, 3552–3559. (b)

(70) Rosu, T.; Pahontu, E.; Pasculescu, S.; Georgescu, R.; Stanica, N.; Curaj, A.; Popescu A.; Leabu, M. Synthesis, Characterization Antibacterial and Antiproliferative Activity of Novel Cu(II) and Pd(II) Complexes with 2-hydroxy-8-R-tricyclo[7.3.1.0.^{2,7}]Tridecane-13-one Thiosemicarbazone. *Eur. J. Med. Chem*. **2010**, *45*, 1627–1634.

(71) Thomadaki, H.; Karaliota, A.; Litos, C.; Scorilas, A. Enhanced Antileukemic Activity of the Novel Complex 2,5-Dihydroxybenzoate Molybdenum(VI) Against 2,5-Dihydroxybenzoate, Polyoxometalate of Mo(VI), and Tetraphenylphosphonium in the Human HL-60 and K562 Leukemic Cell Lines. *J. Med. Chem.*2007**,** *50,* 1316–1321.

(72) (a) Zhang, G.; Ta, C.; Cheng, S.-Y.; Golen, J. A.; Rheingold, A. L. Clicking Thiourea into a Salen Scaffold: Structures and Cytotoxicity of Cobalt(II) and Nickel(II) Complexes. *Inorg. Chem.*

Commun. **2014**, *48*, 127–130. (b) Terenzi, A.; Lotsch, D.; van Schoonhoven, S.; Roller, A.; Kowol, C. R.; Berger, W.; Keppler, B. K.; Barone, G. Another step toward DNA selective targeting: NiII and CuII complexes of a Schiff base ligand able to bind gene promoter G-quadruplexes. *Dalton Trans*. **2016**, *45*, 7758–7767. (c) Herchel, R.; Sindelar, Z.; Travnicek, Z.; Zboril, R.; Vanco, J. Novel 1D Chain Fe(III)-Salen-like Complexes Involving Anionic Heterocyclic N-Donor Ligands. Synthesis, X-ray Structure, Magnetic, 57Fe Mössbauer, and Biological Activity Studies. *Dalton Trans.* **2009**, 9870–9880. (d) Tzubery, A.; Tshuva, E. Y. Cytotoxicity and Hydrolysis of trans-Ti(IV) Complexes of Salen Ligands: Structure–Activity Relationship Studies. *Inorg. Chem.* **2012**, 51, 1796–1804.

(73) Singh, N.; Ranjan, V.; Zaidi, D.; Shyam, H.; Singh, A.; Lodha, D.; Sharma, R.; Verma, U.; Dixit , J.; Balapure, A. K. Insulin Catalyzes the Curcumin-Induced Wound Healing: An In Vitro Model for Gingival Repair. *Indian J. Pharmacol.* **2012**, *44*, 458–462.

(74) Bullock, J. J.; Mehta, S. L.; Lin, Y.; Lolla, P.; Li, P. A. Hyperglycemia-Enhanced Ischemic Brain Damage in Mutant Manganese SOD Mice is Associated with Suppression of HIF-1α. *Neurosci. Lett.* **2009**, *456*, 89–92.

For Table of Contents Only

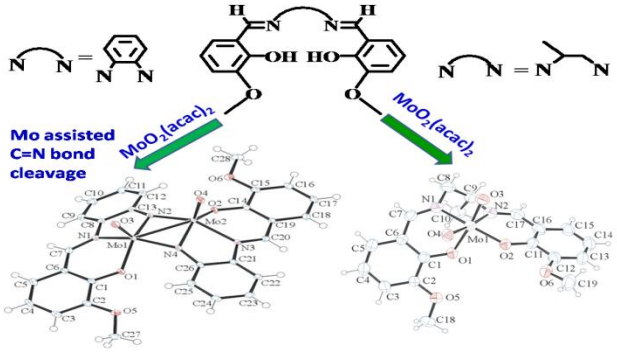

Dimeric bis-μ-imido bridged metal-metal bonded oxidomolybdenum(V) complexes $[Mo_2^{V}O_2L'^{1-4}_2]$ (**1**–**4**) and a new mononuclear dioxidomolybdenum(VI) complex $[Mo^{VI}O_2L^{5}]$ (**5**) synthesized from salen type ligands containing aromatic and aliphatic moieties are reported. $[Mo_2^{V}{}_2L'^{1-4}_2]$ (**1**–**4**) have been furnished by the molybdenum assisted in situ –C=N bond cleavage of one of the imine bonds of the ligands (H_2L^{1-4}) containing aromatic imines. The DNA interactions and the *in vitro* cytotoxic activity of all the complexes have been evaluated.